

## A versatile in situ cofactor enhancing system for meeting cellular demands for engineered metabolic pathways

Jaroensuk, Juthamas; Sutthaphirom, Chalermroj; Phonbuppha, Jittima; Chinantuya, Wachirawit; Kesornpun, Chatchai; Akeratchatapan, Nattanon; Kittipanukul, Narongyot; Phatinuwat, Kamonwan; Hollmann, Frank; More Authors

**DOI**

[10.1016/j.jbc.2023.105598](https://doi.org/10.1016/j.jbc.2023.105598)

**Publication date**

2024

**Document Version**

Final published version

**Published in**

Journal of Biological Chemistry

**Citation (APA)**

Jaroensuk, J., Sutthaphirom, C., Phonbuppha, J., Chinantuya, W., Kesornpun, C., Akeratchatapan, N., Kittipanukul, N., Phatinuwat, K., Hollmann, F., & More Authors (2024). A versatile in situ cofactor enhancing system for meeting cellular demands for engineered metabolic pathways. *Journal of Biological Chemistry*, 300(2), Article 105598. <https://doi.org/10.1016/j.jbc.2023.105598>

**Important note**

To cite this publication, please use the final published version (if applicable).  
Please check the document version above.

**Copyright**




Other than for strictly personal use, it is not permitted to download, forward or distribute the text or part of it, without the consent of the author(s) and/or copyright holder(s), unless the work is under an open content license such as Creative Commons.

**Takedown policy**

Please contact us and provide details if you believe this document breaches copyrights.  
We will remove access to the work immediately and investigate your claim.

# A versatile *in situ* cofactor enhancing system for meeting cellular demands for engineered metabolic pathways

Received for publication, August 17, 2023, and in revised form, December 2, 2023. Published, Papers in Press, December 28, 2023, <https://doi.org/10.1016/j.jbc.2023.105598>

Juthamas Jaroensuk<sup>1,‡</sup>, Chalermroj Sutthaphirom<sup>1,‡</sup>, Jittima Phonbuppha<sup>1</sup>, Wachirawit Chinantuya<sup>1,2</sup>, Chatchai Kesornpun<sup>1</sup>, Nattanon Akeratchatapan<sup>1</sup>, Narongyot Kittipanukul<sup>1</sup>, Kamonwan Phatinuwat<sup>3</sup>, Sopapan Atichartpongkul<sup>4</sup>, Mayuree Fuangthong<sup>3,4</sup>, Thunyarat Pongtharangkul<sup>5</sup>, Frank Hollmann<sup>6</sup>, and Pimchai Chaiyen<sup>1,\*</sup>

From the <sup>1</sup>School of Biomolecular Science and Engineering, Vidyasirimedhi Institute of Science and Technology (VISTEC), Rayong, Thailand; <sup>2</sup>Faculty of Science, Department of Biochemistry and Center for Excellence in Protein and Enzyme Technology, Mahidol University, Bangkok, Thailand; <sup>3</sup>Program in Applied Biological Sciences, Chulabhorn Graduate Institute, Bangkok, Thailand; <sup>4</sup>Laboratory of Biotechnology, Chulabhorn Research Institute, Bangkok, Thailand; <sup>5</sup>Faculty of Science, Department of Biotechnology, Mahidol University, Bangkok, Thailand; <sup>6</sup>Department of Biotechnology, Delft University of Technology, Delft, Netherlands

Reviewed by members of the JBC Editorial Board. Edited by Joseph Jez

Cofactor imbalance obstructs the productivities of metabolically engineered cells. Herein, we employed a minimally perturbing system, xylose reductase and lactose (XR/lactose), to increase the levels of a pool of sugar phosphates which are connected to the biosynthesis of NAD(P)H, FAD, FMN, and ATP in *Escherichia coli*. The XR/lactose system could increase the amounts of the precursors of these cofactors and was tested with three different metabolically engineered cell systems (fatty alcohol biosynthesis, bioluminescence light generation, and alkane biosynthesis) with different cofactor demands. Productivities of these cells were increased 2-4-fold by the XR/lactose system. Untargeted metabolomic analysis revealed different metabolite patterns among these cells, demonstrating that only metabolites involved in relevant cofactor biosynthesis were altered. The results were also confirmed by transcriptomic analysis. Another sugar reducing system (glucose dehydrogenase) could also be used to increase fatty alcohol production but resulted in less yield enhancement than XR. This work demonstrates that the approach of increasing cellular sugar phosphates can be a generic tool to increase *in vivo* cofactor generation upon cellular demand for synthetic biology.

Synthetic biology and metabolic engineering provide greener solutions for the production of valuable chemicals than chemical-based approaches due to their less detrimental effects on the environment (1–3). The approach of using microbial cell factories is also sustainable because it can convert renewable biomass (rather than petrochemicals or other non-renewable resources) into products of interest by fermentations (1, 4–6). However, the productivity of metabolically engineered cells is frequently hampered by the scarcity of substrates or cofactors (e.g., NAD(P)H, FAD, FMN, ATP,

acetyl-CoA) (7–10) required for enzymatic reactions owing to the limited amounts of these compounds available *in vivo*.

A well-established approach to overcome the insufficient supply of cofactors in microbes is the incorporation of extra metabolic pathways for cofactor regeneration (11, 12). For example, formate dehydrogenase or glucose dehydrogenase (GDH) are incorporated into cells to enhance generation of NAD(P)H from NAD(P)<sup>+</sup> using formate and D-glucose as reductants (13, 14), while polyphosphate kinase is used to regenerate ATP from ADP and polyphosphate (7, 15). Although this approach can somewhat enhance regeneration of selected cofactors, it is not entirely efficient because the total amount of cofactors, that is, NAD(P)H plus NAD(P)<sup>+</sup> or ADP plus ATP does not change. Besides, biocatalytic systems often require more than a single cofactor. Developing effective and generic systems to supply all essential cofactors in addition to the main reactions often requires alteration of several genes that are involved in central metabolic pathways, which often leads to changes that are not beneficial for cell fitness (16–18).

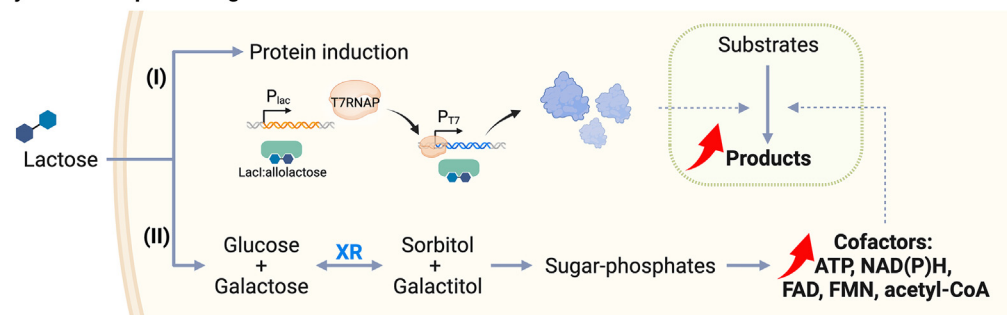
To overcome the challenges mentioned above, we proposed a new and minimally perturbing genetic modification approach for enhancing several cofactor biosynthesis systems in one go by increasing a pool of glycolytic sugar phosphates that are linked directly to the biosynthesis of NAD(P)H, FAD, FMN, ATP, acetyl-CoA. We proposed that expression of only a single gene encoding a sugar reductase to reduce hexoses to hexitols may result in a rewiring of hexitol metabolism, leading to accumulation of sugar phosphates (Fig. 1A), precursors of targeted end-products, and various cofactors. For sugar supply, we wanted to take advantage of a commonly available sugar, lactose, which is routinely used as an inducer for over-expressing heterologous proteins in *Escherichia coli* to supply hexoses (D-glucose and D-galactose). For the choice of sugar reductase, xylose reductase (XR) which is known to reduce several hexoses to generate hexitols was chosen. Although XR was previously applied in engineered microbes to generate

‡ These authors contributed equally to this work.

\* For correspondence: Pimchai Chaiyen, [pimchai.chaiyen@vistec.ac.th](mailto:pimchai.chaiyen@vistec.ac.th).

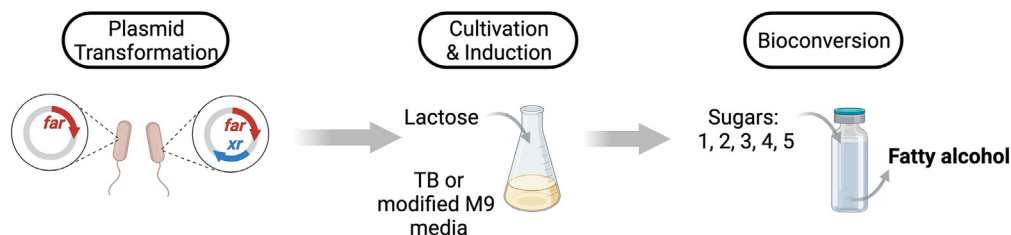
## XR and lactose boost microbial cofactor synthesis

### A System conceptual design

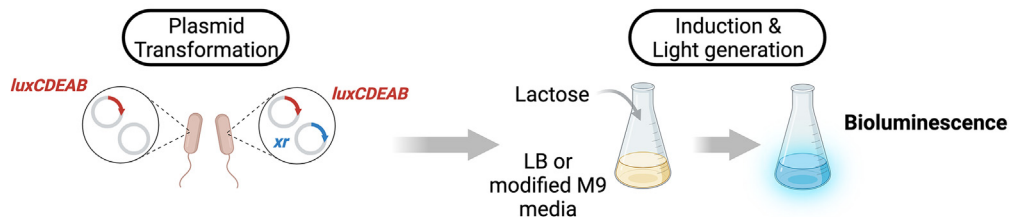


### B Experimental workflow

#### (I) Fatty alcohol biosynthesis



#### (II) Bioluminescence light generation



#### (III) Alkane biosynthesis

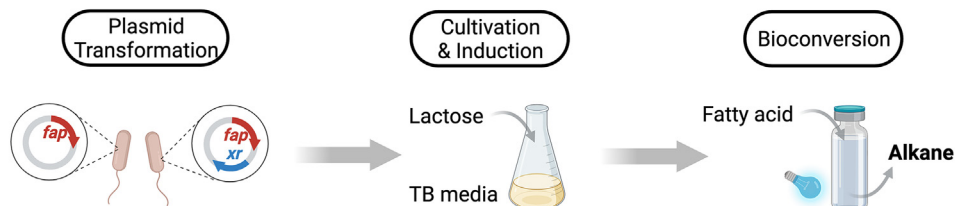


**Figure 1. The concept of XR/lactose and its role in enhancing cofactor synthesis and product yield in engineered cells, along with the associated testing workflow.** A, the conceptual design illustrates the utilization of the XR/lactose system within engineered cells for two primary purposes: (I) inducing enzyme production of the genes under a T7 promoter and (II) enhancing cofactor synthesis to support enzyme activities in the bioconversion step. This enhancement involves utilization of XR to convert glucose and galactose (the breakdown products of lactose) into sugar alcohols. Subsequently, the native metabolisms convert these sugar alcohols into sugar phosphates and other essential cofactors required by the engineered cell. B, the experimental workflow designed to validate the concept described in (A). Three metabolically engineered pathways: (I) fatty alcohol biosynthesis, (II) bioluminescent light generation, and (III) alkane bioproduction were used to showcase the efficiency of the XR/lactose enhancer system. 1, Lactose; 2, D-glucose; 3, D-glucose/D-galactose; 4, D-glucose/D-fructose; 5, D-glucose/L-arabinose. XR/lactose, xylose reductase/lactose.

xylitol from xylose and other pentose sugars (19–21), its use for increasing levels of a pool of sugar phosphates and for enhancing production of cellular cofactors in engineered cells have never been investigated or proposed.

We found that the XR/lactose cofactor boosting system could indeed increase the productivity of three different types of metabolically engineered pathways (fatty alcohol biosynthesis, bioluminescence light generation, and alkane biosynthesis) which demand high usage of cofactors such as NAD(P)H, acetyl-CoA, FAD, FMN, and ATP in *E. coli* BL21 (DE3) by 2–4-fold. We employed metabolomic and transcriptomic

analyses to investigate the metabolic pathways affected by the presence of XR/lactose. The data clearly showed that the XR/lactose boosting system indeed increased levels of intermediates in the sugar phosphate pathways and propagated enhancement effects on key metabolic nodes important for the synthesis of common cellular cofactors such as acetyl-CoA, NAD(P)H/NAD(P), FAD/FMN, and ATP. Notably, the patterns of cofactor enhancement are not the same among the three types of cells investigated but rather customized according to the different demands of the engineered pathways. We further investigated effects of another sugar reductase,

GDH, in a fatty alcohol production system and found similar enhancement effects as XR but with less yield enhancement. Altogether, our work demonstrates that the approach of increasing cellular sugar phosphates can be a generic tool to increase *in vivo* cofactor generation to meet cellular demands.

## Results

### Rationale for system design and selection of XR and lactose as a versatile cofactor booster

Lactose is a natural sugar routinely used as an inducer for overexpressing heterologous proteins in *E. coli* in preparative or industrial scale applications because its cost is markedly cheaper than its analog IPTG, generally used in lab scale applications (6, 22, 23). As lactose is commonly added in surplus amount (typically in 2–20 g/l) to maintain protein overexpression, we thus proposed to take advantage of its excess presence as a resource to supply cofactors *via* the reduction of aldose coupled to the synthesis of sugar phosphates and various cofactor biosynthesis in the engineered *E. coli* (Fig. 1A). When searching for a candidate enzyme to reduce the hydrolyzed products of lactose (D-galactose and D-glucose), XR appeared as an attractive system for performing this task because XR is known to reduce various sugars (24–26). We then tested the activity of the purified XR from *Hypocrea jecorina* in the reduction of glucose and galactose using NADPH. XR from *H. jecorina* was chosen for our study because the enzyme was reported to use not only pentoses (D-xylose, L-arabinose) but also hexoses (D-glucose, D-galactose) as substrates. We found that the enzyme indeed could reduce D-glucose and D-galactose to generate D-sorbitol and D-galactitol (Fig. S1). This is consistent with previous work reporting  $k_{\text{cat}}$  values of  $4.80 \pm 0.20 \text{ s}^{-1}$  for D-glucose and  $1.28 \pm 0.06 \text{ s}^{-1}$  for D-galactose reduction (25). The ability of XR to reduce the two sugars with  $k_{\text{cat}}$  values within a similar range makes the system a suitable fit for our aims.

With the presence of XR and lactose, cells should be able to generate sorbitol and galactitol at comparable rates; these sugar alcohols would then be converted to sorbitol 6-phosphate (S6P) and galactitol 1-phosphate (Gal1P) *via* D-sorbitol and D-galactitol degradation pathways (hexitol degradation pathways), respectively. We hypothesized that when lactose enters the cell, only a fraction of lactose is converted by  $\beta$ -galactosidase to generate allolactose which binds to the repressor protein and triggers *lac* operon expression. The rest of lactose would be hydrolyzed to D-glucose and D-galactose, which in theory can enter the glycolysis and Leloir pathways, respectively. However, because *E. coli* BL21 (DE3) which widely used as a model organism for studying metabolic pathway engineering cannot utilize galactose as a carbon source due to the *gal* mutation (27), the addition of XR provides an additional pathway for the organism to use these hydrolyzed products of lactose efficiently as a resource of cofactors synthesis.

To evaluate the effects of the XR/lactose cofactor boosting system in enhancing the efficiency of biotransformation, we constructed three different *in vivo* biotransformation systems

## XR and lactose boost microbial cofactor synthesis

including fatty alcohol synthesis by fatty acyl-ACP/CoA reductase (FAR), bioluminescence reporter by bacterial luciferase (LuxCDEAB), and alkane synthesis by fatty acid photo-decarboxylase (FAP) (Fig. 1B). These systems were chosen because they use different kinds of cofactors. FAR uses two equivalents of NADPH to convert fatty acyl-ACP/CoA to alcohol (Fig. 2A). LuxAB and LuxCDE generate light upon consumption of FMNH<sub>2</sub>, NAD(P)H, and ATP (Fig. 2B). Different from the other two systems, FAP merely uses FAD as a cofactor and requires external light input to decarboxylate the fatty acid to generate alkane (Fig. 2C).

### Incorporation of the XR/lactose cofactor boosting system increases the productivity of fatty alcohol

Fatty alcohols are important raw chemicals for industries. They are used as co-emulsifiers in cosmetics, fuel, and food and also as starting materials for various reagents (28). A metabolic pathway for fatty alcohol production using the FAR system is shown in Figure 2A. We first tested the ability of the XR/lactose system to boost fatty alcohol production in engineered *E. coli* containing the FAR system (*E. coli-far* and *E. coli-far-xr*). After adding lactose to induce protein overexpression for 6 h, *E. coli-far* and *E. coli-far-xr* were harvested and employed as biocatalysts for fatty alcohol production.

We first evaluated the impact of sugar carbon sources such as lactose, D-glucose, D-glucose/D-galactose, D-glucose/D-fructose, and D-glucose/L-arabinose on fatty alcohol formation. The results show that *E. coli-far-xr* generated more fatty alcohol than *E. coli-far* with all of the sugars tested (Fig. S2). In the scenario where lactose was used for both protein induction and bioconversion, *E. coli-far-xr* generated three times greater fatty alcohol than *E. coli-far* (Fig. 3A). Lactose supplementation at both the protein induction and bioconversion phases resulted in a productivity rate of 165.3  $\mu\text{mol/L/h}$  for *E. coli-far-xr* as compared to 58.1  $\mu\text{mol/L/h}$  for *E. coli-far* (Fig. 3A). The total fatty alcohol titer by this engineered cell using lactose was 0.77 mg/ml or 0.22 g/g lactose equivalent in a batch process. As *E. coli* BL21 (DE3) cannot utilize galactose as a carbon source due to the *gal* mutation (27), it can produce approximately 0.33 g of C16:1 fatty alcohol per gram of lactose as a theoretical yield. Therefore, our fatty alcohol production yield is around 22% of the theoretical yield value for a C16:1 fatty alcohol. It should be noted that our study primarily aims to assess the impact of the enhancer system (XR/lactose) and we have not performed any engineering of other essential metabolic pathways to optimize the yield of fatty alcohol conversion.

We also demonstrated the feasibility of using the XR/lactose system when culturing biocatalysts in the modified M9 media (details in Experimental procedures). The results showed similar outcomes as those using rich media (Fig. 3B). Using the modified M9 media, total fatty alcohol produced from *E. coli-far-xr* was 3.8-fold higher than that from *E. coli-far*. This data illustrates the feasibility of using the XR/lactose system in various media which should be useful for future application in scaling up of production processes.

## XR and lactose boost microbial cofactor synthesis

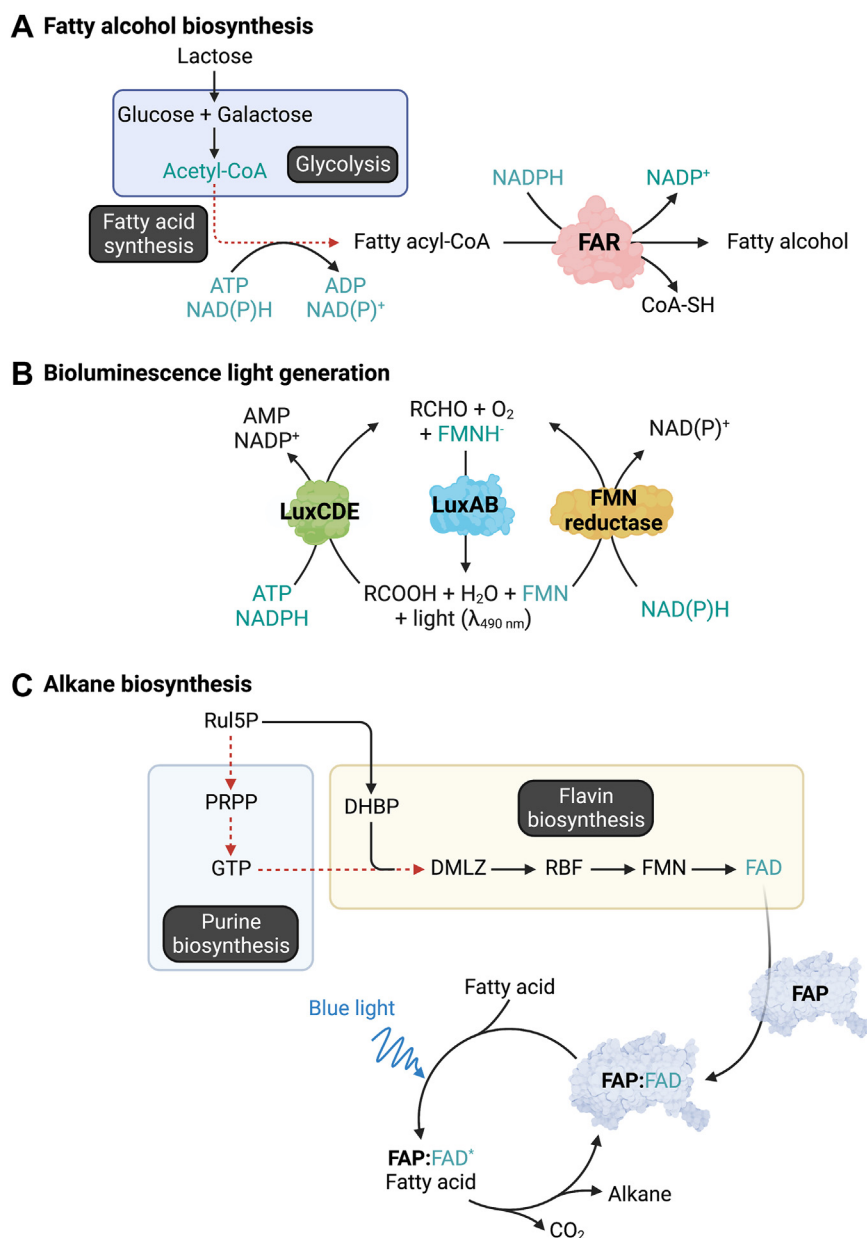


**Figure 2. The metabolic pathways of engineered cells for XR/lactose system testing.** A, pathway of fatty alcohol biosynthesis from sugar (e.g., lactose) by fatty acyl-ACP/CoA reductase (FAR). FAR utilizes NADPH to convert fatty acyl-ACP/CoA, an intermediate in fatty acid synthesis, to yield fatty alcohol. B, the catalytic cycle of complete bacterial luciferase (LuxAB)/acid reductase (LuxCDE)/flavin reductase cascades. C, pathways involved with FAD synthesis and the catalytic cycle of alkane biosynthesis by fatty acid photodecarboxylase (FAP). The reaction requires blue light (450 nm) to activate FAD at the enzyme active site for decarboxylation of fatty acid substrates to form alkanes and CO<sub>2</sub>. XR/lactose, xylose reductase/lactose.

### The XR/lactose system increases the level of sugar phosphates which enhanced production of acetyl-CoA, ATP, and NADPH required for the fatty alcohol biosynthesis

As the fatty alcohol production by FAR requires two equivalents of NADPH (four electrons reduction process) to reduce fatty acyl-ACP/CoA, an intermediate of the fatty acid synthesis pathway, we hypothesized that the increase of fatty alcohol production might be due to the increase in fatty acyl-ACP/CoA, precursors of fatty acid biosynthesis, and cofactors involved in the fatty acid biosynthesis process including NADPH, ATP, and acetyl-CoA (Fig. 2A). We then performed untargeted metabolomics analysis of *E. coli-far-xr* and *E. coli-far* cells to compare the differences in their metabolites after

1.5 h of lactose bioconversion to fatty alcohol. These data would present snapshots at early time points of cell metabolite levels and the activities of enzyme networks involved in the fatty alcohol biosynthesis process. Differences observed between *E. coli-far-xr* and *E. coli-far* cells would indicate changes due to aldose reduction and verify whether the addition of XR could enhance the biosynthesis of sugar phosphates and the biosynthesis of related cofactors.

We performed untargeted metabolomic analysis to identify compounds for which their abundance was different among the two strains. Principal component analysis (PCA) was employed to initially visualize metabolomic data sets. The data clearly showed that the presence of XR indeed caused global



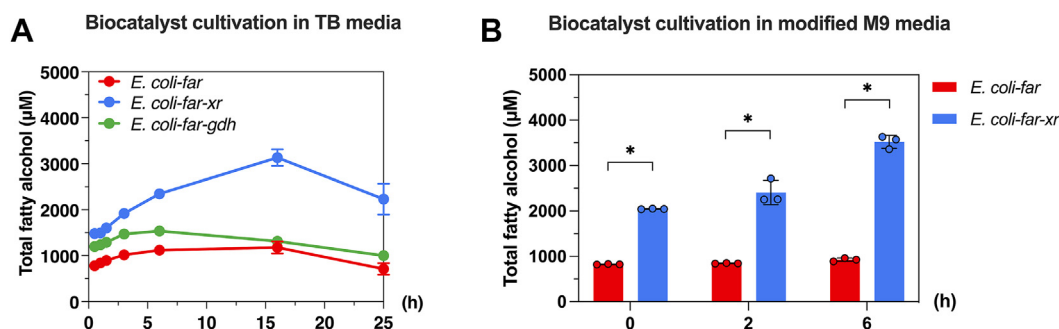


**Figure 3. Fatty alcohol production from the FAR-engineering *Escherichia coli* with and without XR cofactor enhancement.** A, production of total fatty alcohol from 10 mM lactose in 0.1 M potassium phosphate buffer at pH 7.5 by *E. coli-far* (red), *E. coli-far-xr* (blue), and *E. coli-far-gdh* (green) grown in TB media. Data are shown as mean  $\pm$  s.d.,  $n = 3$  replicate cultures. B, production of fatty alcohol from 10 mM lactose in 0.1 M potassium phosphate buffer at pH 7.5 by *E. coli-far* (red) and *E. coli-far-xr* (blue) when the biocatalysts were cultured in modified M9 media (M9 salt + 33 mM thiamine, 0.1% (w/v) casamino acids, 0.2% (v/v) glycerol). Data are shown as mean  $\pm$  s.d.,  $n = 3$  replicate cultures; the asterisks denote significant differences as determined by multiple  $t$  test ( $p < 0.05$ ).

metabolic changes in *E. coli-far* (Fig. 4A). Using unpaired and univariate analyses, we found 234  $m/z$  features from a total of 1250  $m/z$  features whose fold-changes (FC) were larger than 1.5 ( $p < 0.05$ ) (Fig. 4B), and 90 out of 234 features could be annotated (Table S1). The annotated metabolites that displayed significantly different fold-changes were indeed connected to metabolic pathways of sorbitol, galactitol, glycolysis, pentose-phosphate pathway (PPP), phosphopantothenate, CoA biosynthesis, and fatty acid synthesis. In addition, we also found an increase of compounds involved with trehalose biosynthesis and glutathione production (Table S1).

To fully understand the changes of metabolites across the pathways involved, we plotted fold-changes ( $\log_2$  FC) of certain metabolites and presented the data based on the magnitude of the  $\log_2$  FC (Fig. 4C). The time-course data showed that at the beginning of the bioconversion, the levels of acetyl-CoA, ATP, and NADPH that are necessary for the synthesis of fatty acid and fatty alcohol were clearly increased in *E. coli-far-xr* as compared to *E. coli-far*, with a FC  $> 1.5$  ( $p < 0.05$ ) (Fig. 4C). Although the amount of these metabolites reduced as the bioconversion progressed, their levels were still greater than those of *E. coli-far* (Fig. 4D).

The time course analysis of sugar substrates (lactose and its hydrolyzed products) during the bioconversion reaction revealed that in *E. coli-far*, the hydrolyzed product of lactose, D-galactose, accumulated both extracellularly and intracellularly over time (Fig. 5A). In contrast, *E. coli-far-xr* exhibited a reduced accumulation of D-galactose over the same period (Fig. 5B). Notably, both cell types exhibit similar rates of D-glucose consumption (Fig. 5, A and B). Furthermore, trace amounts of D-sorbitol/D-galactitol were detected intracellularly only in *E. coli-far-xr*; however, these compounds remained undetectable by the end of the bioconversion process (Fig. 5C). These data suggest that the *E. coli-far-xr* reduced glucose and galactose to form sorbitol and galactitol which were then phosphorylated and entered the central carbon metabolisms in the forms of sugar phosphates, S6P and Gal1P, respectively. As shown in Figure 4C, the increase of S6P, Gal1P, and tagatose 1,6-bisphosphate into glycolysis can directly elevate the level of the glycolytic metabolites, 3-phosphoglycerate (3-PG), and the

PPP metabolites such as 6-phosphogluconic acid (6-PG), which would allow greater production of acetyl-CoA, ATP, and NADPH to support fatty acid and fatty alcohol synthesis by the FAR system. Furthermore, time-course analysis of metabolites related to fatty alcohol synthesis at 1.5 h, 3 h, and 6 h revealed that *E. coli-far-xr* generated substantially more (R)-pantoate, 3-PG, and 6-PG than *E. coli-far* (Fig. 4D), indicating that *E. coli-far-xr* has greater precursors for synthesis of CoA, acetyl-CoA, and energy-related metabolites of cofactors than *E. coli-far*.

Interestingly, we also detected the up-regulation of glutathione (GSH) and trehalose 6-phosphate, an intermediate of trehalose biosynthesis, in *E. coli-far-xr* (Fig. 4C). Trehalose and GSH are known to facilitate bacterial adaptability to tolerate oxidative stress (29) and osmotic stress (30–32), as the over-expression of GSH-encoding genes in *Clostridium acetobutylicum* was shown to improve the strain tolerance to solvent and increase 1-butanol production (33). We thus explored the tolerance of *E. coli-far* and *E. coli-far-xr* to H<sub>2</sub>O<sub>2</sub> (oxidative stressor) and NaCl (osmotic stressor), respectively. We found that *E. coli-far-xr* showed higher cell viability than *E. coli-far* after exposure to 5 mM H<sub>2</sub>O<sub>2</sub> but the tolerance towards 5% (w/v) NaCl was similar for these two cell types (Fig. S3). Therefore, the *E. coli-far-xr* system which has a greater carbon flow into central metabolism pathways than *E. coli-far* without XR can increase the synthesis of GSH, which gives it an extra advantage to improve cellular resistance to oxidative stressors during the fatty alcohol bioconversion process.

#### Enhancement of fatty alcohol production by GDH in comparison to XR

To investigate whether another sugar reductase such as GDH can also be used as a cofactor enhancing system as XR, we constructed the system of *E. coli-far-gdh* in which GDH was used as a sugar reductase and investigated fatty alcohol production in comparison to the *E. coli-far-xr* system. Both lactose and D-glucose were tested as carbon sources for sugar alcohol production by GDH. The results showed that GDH could also increase the overall fatty alcohol production ( $\sim 1.2$

# XR and lactose boost microbial cofactor synthesis

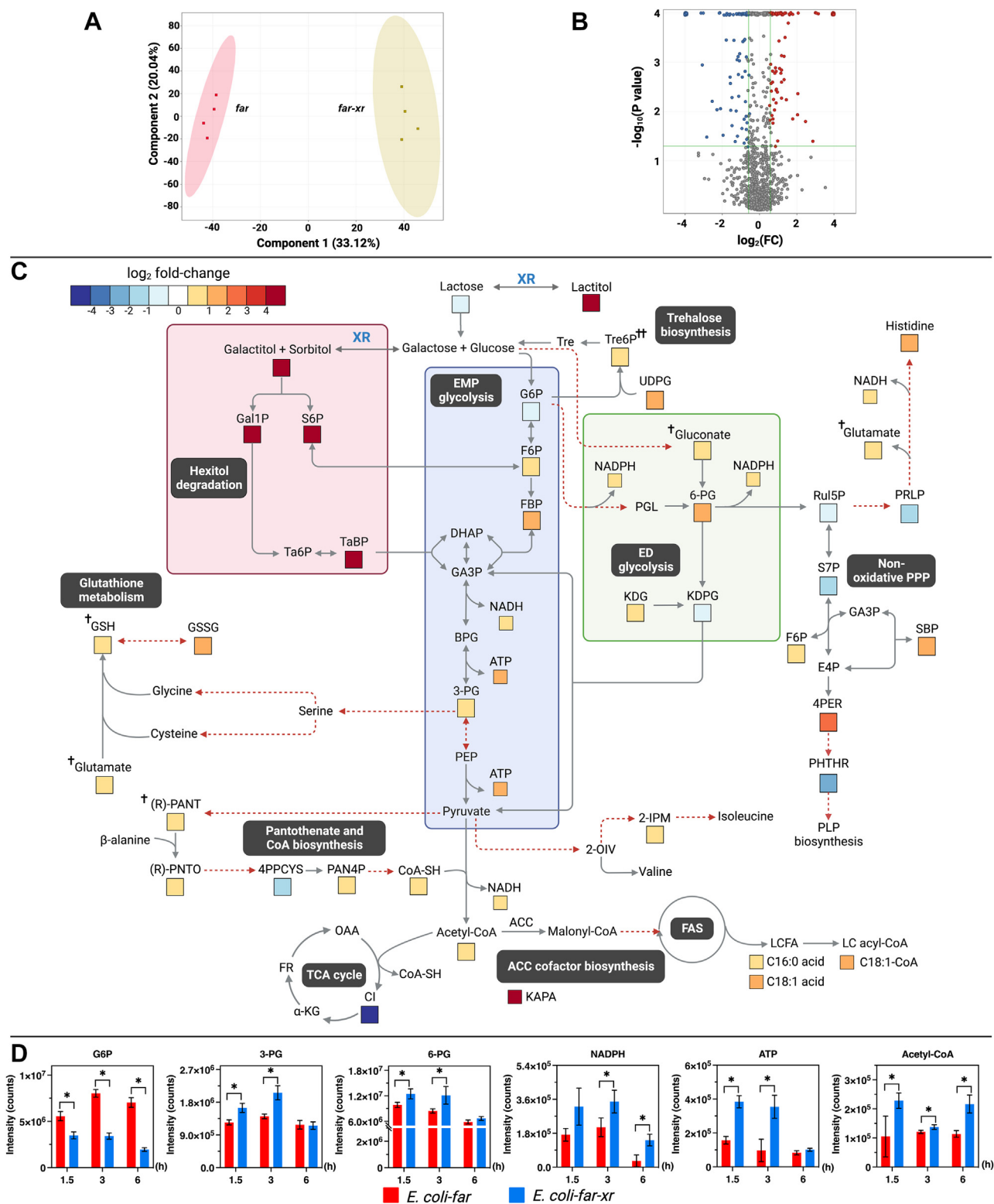


**Figure 4. Untargeted metabolomic analysis from the FAR-engineering *Escherichia coli* with and without XR cofactor enhancement.** *A*, principal component analysis (PCA) score plots of the first two components show distinct separation of metabolites produced by *E. coli-far* and *E. coli-far-xr*. Data represent averages from four replicate cultures. *B*, a volcano plot of metabolites of *E. coli-far-xr* versus *E. coli-far* after 1.5 h of the bioconversion process. Red represents the upregulated metabolites; blue represents the downregulated metabolites of *E. coli-far-xr* compared to those of *E. coli-far* ( $FC > 1.5$ ,  $p < 0.05$ ). Gray represents the metabolites for which the levels are not different between *E. coli-far* and *E. coli-far-xr*. *C*, map of the metabolite changes at 1.5 h after the start of fatty alcohol bioconversion. The  $\log_2$  FC for each metabolite in *E. coli-far-xr* compared to *E. coli-far* whose FC  $> 1.5$  ( $p < 0.05$ ) are represented according to the color scale. † Denoting metabolites for which FC  $> 1.2$  ( $p < 0.05$ ); †† denoting metabolites for which FC  $> 1.2$  ( $p < 0.1$ ). *D*, time-course analysis of metabolites during the bioconversion process. Data are shown as mean  $\pm$  s.d.,  $n = 4$  replicate cultures; asterisks denote significant differences by multiple  $t$  test ( $p < 0.05$ ). FAR, fatty acyl-CoA reductase.

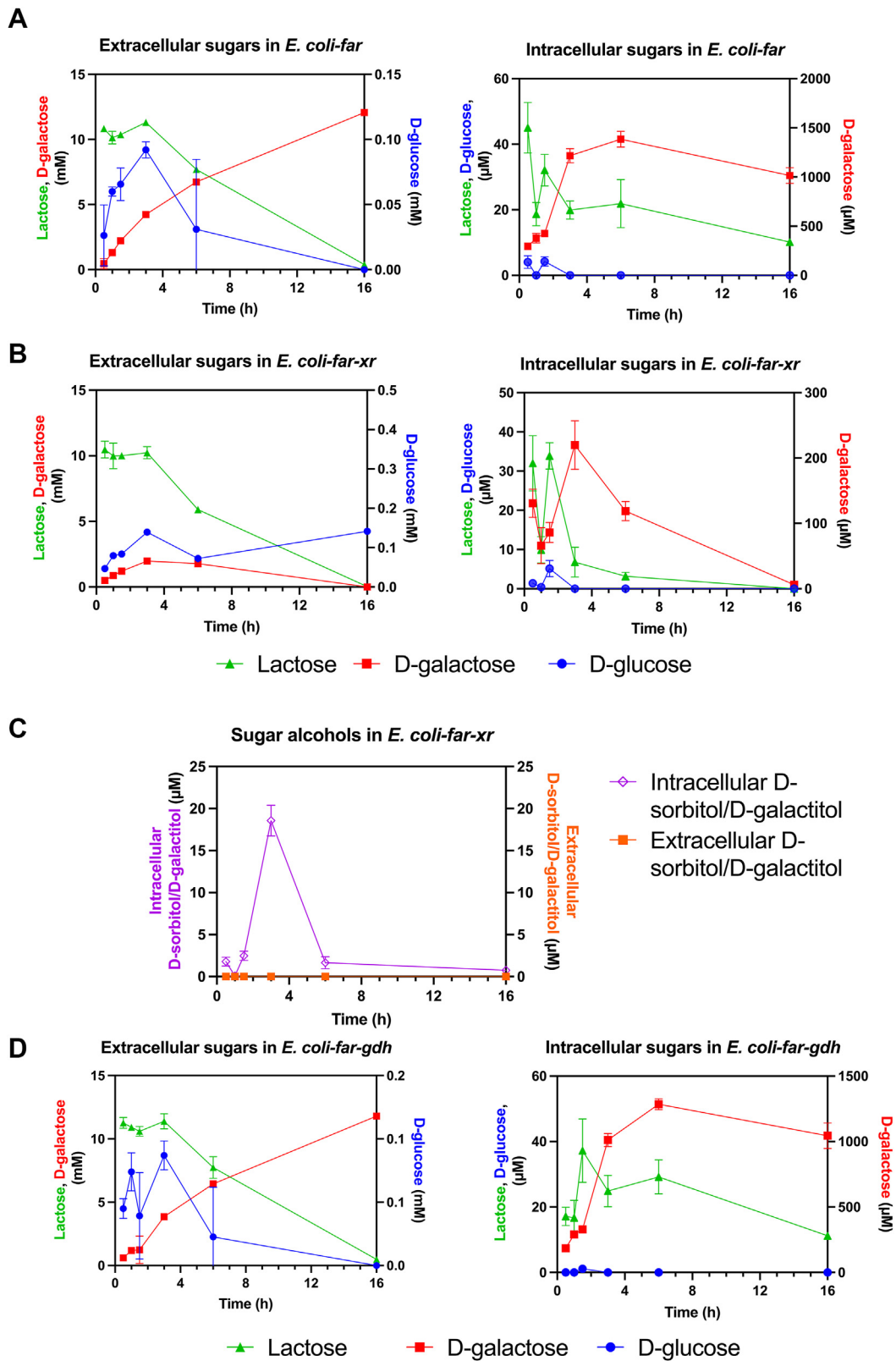


**Figure 5. Comparison of the amount of sugars and sugar alcohol in the bioconversion by different cofactor regenerating systems in the engineered cell.** Lactose (green), D-glucose (blue), D-galactose (red), and D-sorbitol/D-galactitol (purple for intracellular and orange for extracellular) were detected during the bioconversion in *E. coli-far* (A), *E. coli-far-xr* (B and C), *E. coli-far-gdh* (D) when 10 mM lactose was used as a substrate. The bioconversion was described in the [Experimental procedures](#). These graphs show the sugars from both inside the cell and those secreted into media over time. Extracellular sorbitol/galactitol was not found in all samples. Analytical methods were described in the [Experimental procedures](#) section. Data are shown as mean  $\pm$  s.d.,  $n = 3$  replicate cultures. FAR, fatty acyl-CoA reductase.



## XR and lactose boost microbial cofactor synthesis

fold in the presence of lactose (Fig. 3A) and about 2-fold in the presence of D-glucose (Fig. S4). However, the enhancement effects in fatty alcohol production by the *E. coli-far-gdh*/lactose and *E. coli-far-gdh*/D-glucose systems were significantly less than those of the XR/lactose system which was about 3-fold increment (Fig. S4). One possible explanation for the difference in product enhancement between XR and GDH is that GDH does not facilitate the consumption of D-galactose. This is supported by the observed accumulation of D-galactose throughout the bioconversion process when lactose was used as the substrate in *E. coli-far-gdh* (Fig. 5D). In contrast, in the presence of XR, there was a significantly reduced accumulation of D-galactose, both extracellularly and intracellularly compared to *E. coli-far* and *E. coli-far-gdh* (Fig. 5).

### Transcriptomics of genes related to sugar catabolisms of *E. coli-far-xr*

All results shown above clearly indicate that the XR/lactose system could increase levels of sugar alcohol and sugar phosphates, resulting in the enhancement of production of various cofactors (Fig. 4). We then further investigated expression levels (transcriptomics analysis) of genes involving in the early phase of sugar catabolisms where metabolites were shown to be increased in the *E. coli-far-xr* cell. Cells at the time point of 60 min which should be correlated with metabolites profiles at the time point of 90 min shown in Figure 4C were collected for analysis. Results in Figure 6 showed that the genes related to gluconate metabolisms (linked to Entner-Doudoroff (ED)) and PPP in *E. coli-far-xr* were clearly upregulated such as the glucose-6-phosphate dehydrogenase (*zwf*) and the gluconate kinase (*gntK*) genes which are related to the synthesis of 6-PG. The upregulated level of *gntK* is probably linked to the active PPP pathway in *E. coli-far-xr* in which the flux via ribulose-5-phosphate was drawn due to the upregulation of histidinol-phosphate aminotransferase (*hisC*) (Fig. 6). The upregulation of *hisC* would increase the synthesis of histidinol, a precursor of histidine synthesis; this result agreed well with the increased level of histidine shown in Figure 4C. Similarly, the transcriptomic results can also explain the increased levels of sedoheptulose 1,7-bisphosphate and O-phospho-4-hydroxy-L-threonine (Fig. 4C) which originated from precursors in the PPP pathway.

Remarkably, the acetyl-CoA synthase gene (*aceE*) was upregulated 9-fold, explaining the increased levels of acetyl-CoA (Fig. 4D). The genes involved in the synthesis of cysteine and glutathione (*cysK*, *gshB*, *gor*) were also greatly increased (2–8 folds), in agreement with the increased levels of glutathione observed (Figs. 4C and 6). Altogether, the data from the transcriptomic analysis are in agreement with the metabolomic data and could explain the links between the increased levels of D-sorbitol, D-galactitol, and sugar phosphates to various pathways leading to synthesis of key metabolites in *E. coli*.

### Incorporation of the XR/lactose cofactor boosting system enhances light generation by bacterial luciferase

To further test the generality of XR/lactose in enhancing cofactors synthesis in other metabolic engineering pathways,

we investigated whether XR/lactose could enhance *in vivo* bacterial bioluminescence catalyzed by three enzymatic reactions including those of bacterial luciferase (LuxAB), acid reductase (LuxCDE), and flavin reductase (Fig. 2B). Flavin reductase generates reduced FMN (FMNH<sup>-</sup>) by reducing FMN using NAD(P)H, while LuxCDE reduces a long chain fatty acid using NADPH and ATP to generate an aldehyde substrate. LuxAB oxidizes a long chain aldehyde to generate acid with concomitant light emission (34). Because this bioreporter system continuously consumes NADPH and ATP to generate light, it provides a good opportunity for testing the ability of the XR/lactose to boost up and supply cofactors to enhance light production.

The results clearly indicate that bioluminescence generated from *E. coli-luxCDEAB-xr* is indeed brighter and lasts longer than that from *E. coli-luxCDEAB* (Fig. 7A). The light signal from *E. coli-luxCDEAB-xr* remained after 24 h and exhibited >4-fold enhancement at that period compared to that of *E. coli-luxCDEAB*.

We also demonstrated the ability of the XR/lactose system to enhance bioluminescence in a modified M9 media. The results showed that the XR/lactose system could also enhance and prolong the cell brightness in the modified M9 media as well (Fig. 7B). We thus investigated the change of metabolites in these cells in the following section.

### The XR/lactose cofactor boosting system enhances light production via increased FMN, ATP and NAD(P)H

To understand the molecular mechanisms of bioluminescence enhancement by the XR/lactose boosting system, we performed untargeted metabolomic analysis to compare the difference in metabolite levels between *E. coli-luxCDEAB* and *E. coli-luxCDEAB-xr*. For a time-point of investigation, we chose to investigate the cells after 24 h of light generation because it was a period where *E. coli-luxCDEAB-xr* showed the greatest difference in light signals. Details of methodology are described in Experimental procedures and the overall analysis protocols were similar to those previously described for fatty alcohol production.

The results of PCA analysis of metabolites derived from *E. coli-luxCDEAB* and *E. coli-luxCDEAB-xr* can be clearly grouped according to each cell type (Fig. 8A). Using unpaired and univariate analyses, we found 353 *m/z* features from a total of 1269 *m/z* features whose FC > 1.5 ( $p < 0.05$ ) (Figs. 8B), and 93 of the 353 *m/z* features could be annotated (Table S2). Consistently, metabolites altered were mostly similar to those pathways observed in fatty alcohol production shown in Figures 4C and 8C. Interestingly, we also found additional altered pathways in bioreporter cells including biosynthesis of FMN, folate biosynthesis, purine and pyrimidine, and peptidoglycan (Fig. 8C).

Comparison of levels of intracellular metabolites of the two prototype cells using the fold-change analysis showed that *E. coli-luxCDEAB-xr* has higher levels of metabolites related to biosynthesis pathways for production of NADPH (FC > 1.2,  $p < 0.1$ ) and FMN (FC > 2,  $p < 0.05$ ) than those of *E. coli-*

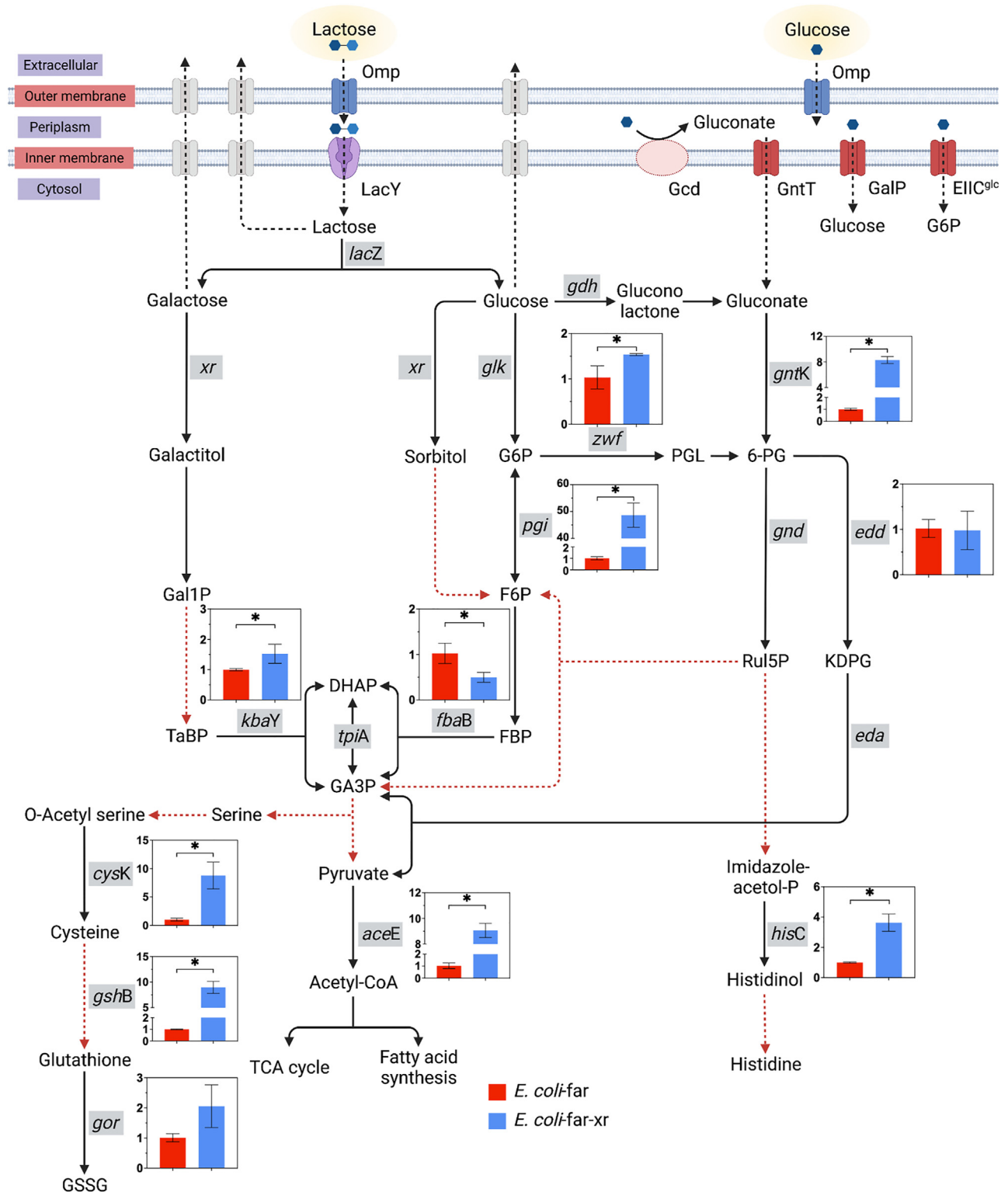


**Figure 6. Transcriptomics of sugar catabolism in XR-incorporated cells.** Expression levels of genes related to lactose and glucose catabolisms in *E. coli-far* and *E. coli-far-xr* are represented by red and blue bars, respectively. Y-axis of each bar graph refers to the relative quantification (RQ). Genes encoding for enzymes catalyzing relevant steps are labeled in rectangular gray boxes. Black dashed lines indicate sugar metabolic routes. Red dashed lines represent pathways in which multiple enzymatic cascades are possible. Data are shown as mean  $\pm$  s.d., n = 3 replicate cultures; asterisks denote significant differences by multiple *t* test ( $p < 0.05$ ).

*luxCDEAB* (Fig. 8, C and D). Here, we could not observe ATP; this might be due to the rate of ATP utilization being much greater than the rate of production, causing the level of ATP to

be lower than the detection limit of the high-resolution mass spectrometer (IM-QTOF, LC-MS system). We thus used triple quadrupole mass spectrometry operating in selective ion

## XR and lactose boost microbial cofactor synthesis

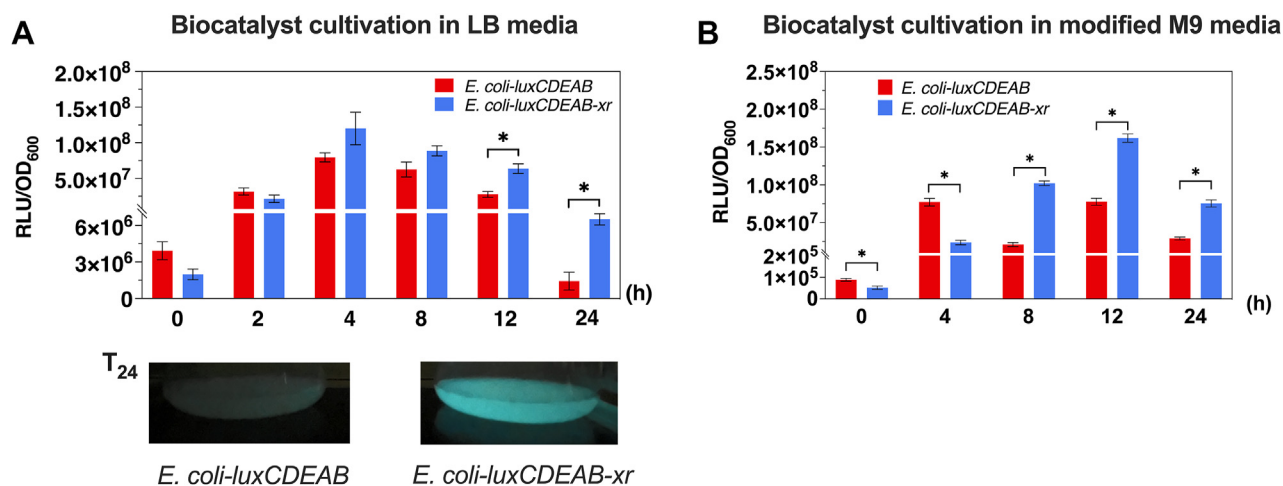


**Figure 7. Bioluminescence generation of the bioluminescence bioreporter cells.** The bioluminescence generated from *E. coli-luxCDEAB* and *E. coli-luxCDEAB-xr* in LB media (A) and modified M9 media (B) containing 10 mM lactose. Data are shown as mean  $\pm$  s.d.,  $n = 3$  replicate cultures; asterisks denote significant differences by multiple  $t$  test ( $p < 0.05$ ). The photos below are culture solutions of the luminous *E. coli-luxCDEAB* (left) and *E. coli-luxCDEAB-xr* (right) grown at 25 °C for 24 h in LB media supplemented with 10 mM lactose. The photo was taken in the dark.

monitoring mode for targeted analysis and could observe that the level of ATP in *E. coli-luxCDEAB-xr* was 2-fold higher than that of *E. coli-luxCDEAB* at 12 h and 24 h of light generation (Fig. S5). The metabolomic data shown in Figure 8C also demonstrate that the light enhancement is likely due to the increase of S6P and Gal1P, which are directly linked to the increased levels of NADPH and FMN. The decrease in the level of G6P, a branch metabolite from glycolysis, and PPP was observed, indicating that G6P was heavily consumed by the *E. coli-luxCDEAB-xr* for creating NADPH and FMN. The increased presence of these metabolites can be used in the bioluminescence catalytic cascade and thus enhances bioluminescence light generation.

High detected concentrations of metabolites in folate biosynthesis such as 5-methyltetrahydrofolate (5-MeTHF) was in agreement with the high levels of NAD(P)H and FMN, indicating that PPP is highly active in the XR-incorporated biocatalyst which is due to the increase in G6P flow into the PPP biosynthesis (Fig. 8C). 5-MeTHF is necessary for production of a number of cellular components such as thymidylate, pantothenate, and purine nucleotides. The increased level of 5-MeTHF possibly results in the observed up-regulation of acetyl-CoA, fatty acid, purine and pyrimidine, and peptidoglycan biosynthesis in *E. coli-luxCDEAB-xr* shown in Figure 8C. These compounds are important for the synthesis of cellular components during growth, thus enhancing prolonged and brighter light production signals.

A time-course analysis of metabolites obtained from *E. coli-luxCDEAB-xr* and *E. coli-luxCDEAB* cells after addition of lactose for 4, 8, 12, and 24 h revealed the decreased levels of G6P in *E. coli-luxCDEAB-xr*, suggesting a fast conversion of this sugar phosphate into the PPP pathway which helps prolong bioluminescence production. The brighter light of *E. coli-luxCDEAB-xr* than that of *E. coli-luxCDEAB* was also supported by the higher levels of FMN and NADPH in *E. coli-luxCDEAB-xr* than those of *E. coli-luxCDEAB* throughout 4 to 24 h (Fig. 8D). Altogether, these results agree well with the

fatty alcohol production system in that the XR/lactose system can boost generation of cofactors required by the engineered metabolic pathway, including NAD(P)H, ATP, and acetyl-CoA.

### Incorporation of XR/lactose enhances the alkane production rate

The third system we used for testing cofactor boosting effects of XR/lactose was FAP, a flavoenzyme catalyzing photodecarboxylation of fatty acids to produce hydrocarbons. As illustrated in Figure 2C, this enzyme requires photons from blue light (400–520 nm) to activate its FAD cofactor for catalysis. Our results showed that the combined use of FAP and XR led to an improvement in the *in vivo* production of alkane from exogenous fatty acid in both two different systems of XR expression, genomically-integrated, and plasmid expression (Fig. 9A and S6). For the genome-integrated XR, we found a 1.6-fold improvement of *in vivo* production of tridecane from exogenous tetradecanoic acid by *E. coli-fap-xr* compared to *E. coli-fap*. The production rate was increased from 0.8 mmol/L/h to 1.3 mmol/L/h (Fig. 9A) and the period required for completing the reaction by the FAP-XR system was much shorter than that of the system without XR. As FAD is a key cofactor in photodecarboxylation by FAP, we hypothesized that co-expression of XR enhances riboflavin synthesis, which in turn increases the level of FAD-bound FAP.

### XR accelerates alkane production rate by increasing the formation of FAD in *E. coli*

Because the addition of XR increases the rate of alkane production of *E. coli* harboring FAP, we employed untargeted metabolomics analysis to investigate the function of XR in this biocatalyst and during the bioconversion process. We found that XR altered the flavin biosynthesis pathways, resulting in the higher level of FAD in *E. coli-fap-xr* compared to that in *E. coli-fap* (Fig. S7). Analysis of *E. coli-fap-xr* and *E. coli-fap*

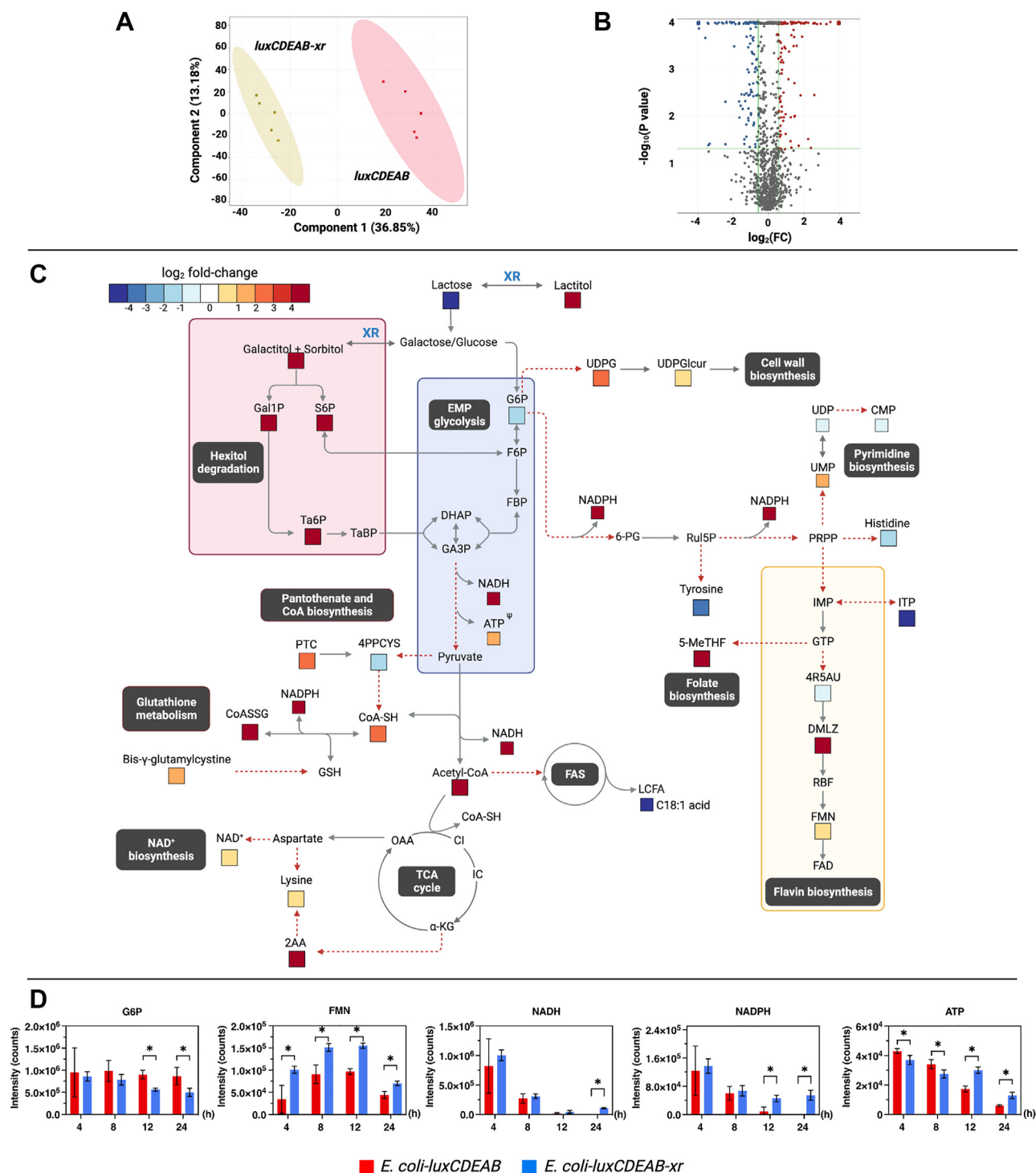


**Figure 8. Untargeted metabolomics analysis from the bioluminescence bioreporter cells.** A, principal component analysis (PCA) score plots of metabolite levels of *E. coli-luxCDEAB* and *E. coli-luxCDEAB-xr* after 24 h of bioluminescence generation. PCA of the first two components shows distinct separation of variances which indicate the influence of the types of metabolites produced by *E. coli-luxCDEAB* and *E. coli-luxCDEAB-xr*. Data are shown as mean  $\pm$  s.d.,  $n = 5$  replicate cultures. B, volcano plots of metabolites in *E. coli-luxCDEAB* and *E. coli-luxCDEAB-xr* cells at 24 h after bioluminescence generation. Red represents the upregulated metabolites, while blue represents the downregulated metabolites as compared to *E. coli-luxCDEAB* ( $\text{FC} > 1.5$ ,  $p < 0.05$ ). Gray represents metabolites which are not different between *E. coli-luxCDEAB* and *E. coli-luxCDEAB-xr*. C, map of the metabolic changes in bioluminescent cells after adding lactose for 24 h. The  $\log_2$  FC for each metabolite in *E. coli-luxCDEAB-xr* versus *E. coli-luxCDEAB* whose  $\text{FC} > 1.5$  ( $p < 0.05$ ) are displayed according to the color scale. <sup>ψ</sup> Denoting the level of metabolites derived from LC/MS QQQ analysis. D, time-course analysis of metabolites after adding 10 mM lactose. Data are shown as mean  $\pm$  s.d.,  $n = 5$  replicate cultures; the asterisks denote significant differences as determined by multiple  $t$  test ( $p < 0.05$ ).



## XR and lactose boost microbial cofactor synthesis

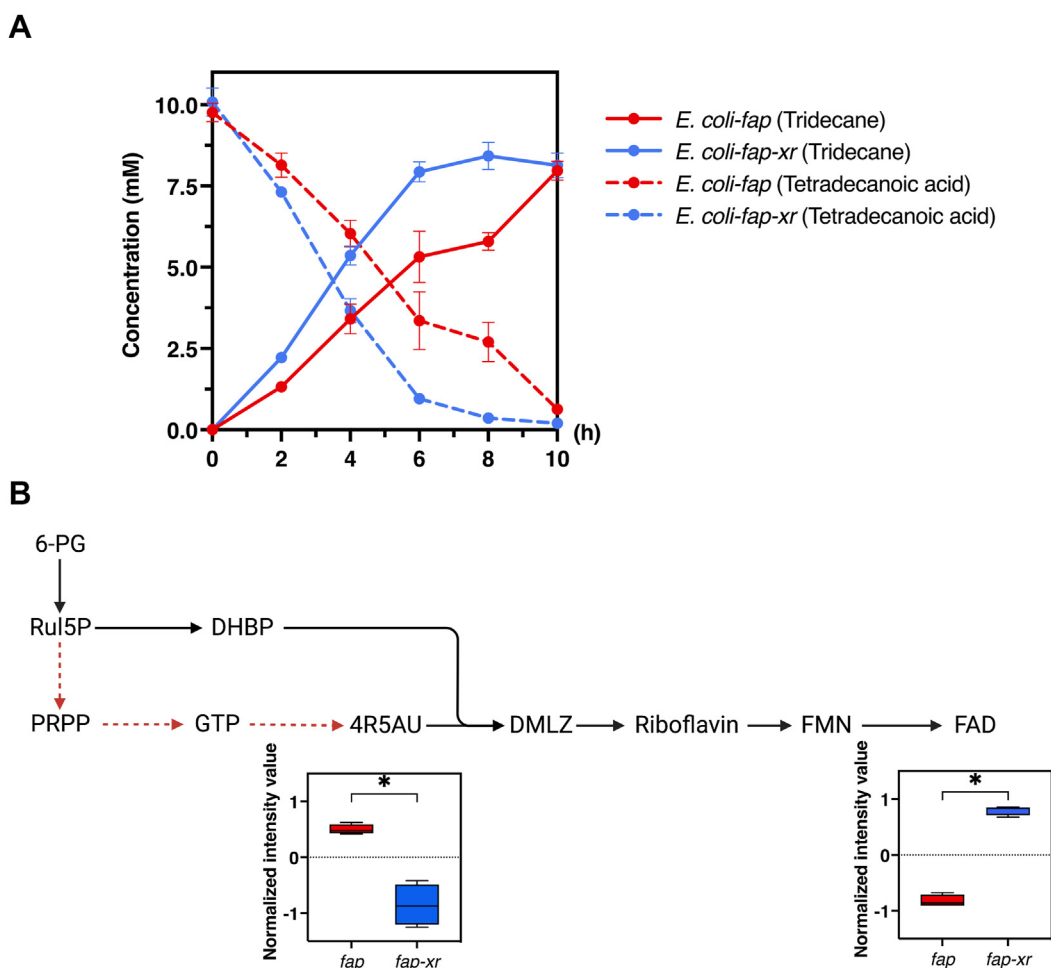


**Figure 9. Alkane biosynthesis by fatty acid photodecarboxylase.** A, production of alkane from fatty acid by *Escherichia coli* harboring *Cvfap*. Tridecane production by *E. coli-fap* is indicated by the red-solid line and production by *E. coli-fap-xr* is indicated by the blue-solid line. Utilization of tetradecanoic acid by *E. coli-fap* is shown as the red-dashed line and *E. coli-fap-xr* as the blue-dashed line. The bioconversion processes were carried out in 0.1 M potassium phosphate buffer containing 10 mM tetradecanoic acid. Data are shown as mean  $\pm$  s.d.,  $n = 4$  replicate cultures. B, comparison of intracellular flavin-related metabolites after 5 h of alkane bioconversion. Levels of metabolites were normalized by total abundance from four replicates and represented in a box-whisker plot. The asterisks denote significant differences as determined by a multiple  $t$  test ( $p < 0.05$ ).

cells after 5 h of the bioconversion process, at which point the alkane productivity was increased the most, revealed that the difference between these two cell types indeed lies mostly in the series of metabolites involved in FAD biosynthesis (Table S3). The intracellular concentration of 5-amino-6-(1-D-ribylamino) uracil (4R5AU), an intermediate of flavin biosynthesis, was less accumulated in *E. coli-fap-xr* than in *E. coli-fap*, and the level of 4R5AU in *E. coli-fap-xr* was 2.5-fold lower ( $p < 0.05$ ) than that of *E. coli-fap* (Fig. 9B). However, *E. coli-fap-xr* had a level of FAD 3-fold higher ( $p < 0.05$ ) than that of *E. coli-fap* (Fig. 9B). These data implied that the FAD biosynthesis in *E. coli-fap-xr* was more active than that of *E. coli-fap*, resulting in higher amounts of the active biocatalyst, FAD-bound FAP, for catalyzing the conversion of fatty acid to alkane. Confirmed by the whole-cell bioconversion data, *E. coli-fap-xr* showed a higher rate of bioconversion than *E. coli-fap* (Fig. 9A).

The increased rate of alkane bioconversion by *E. coli-fap-xr* allows a shorter light exposure time for the bioconversion process. This would allow the system to gain higher efficiency

in alkane production because FAP can be inactivated by radical mechanisms after prolonged light exposure (35). In the past, several methods have been attempted to maintain bioconversion by prolonging the substrate incorporation step to increase the FAP stability (36) or supplying new active cells to the reactor (37, 38). With the XR/lactose boosting system, the alkane production by FAP can be enhanced using a simple method.

## Discussion

The results presented here demonstrated the efficient use of XR/lactose as a simple tool to supply various cofactors in *E. coli* for enhancing product formation by metabolically engineered cells requiring different quantities of cofactors (e.g., acetyl-CoA, NAD(P)H, ATP, and FAD/FMN). Our results showed that XR/lactose had a strong capability to drive metabolically engineered cells in two settings: (i) in the multi-step bioconversion, in which engineered cells require a steady supply of cofactors throughout the process and (ii) in the



single-step bioconversion in which the engineered cells only require a cofactor for producing an active protein. Another interesting aspect of the XR/lactose system is that the changes of metabolites are not the same for all systems; the metabolic flux appeared to change according to the systems' particular demand.

For the multi-step bioconversion, the data herein showed the effectiveness of XR/lactose in boosting the production of fatty alcohol and light. By using the XR/lactose system, the fatty alcohol-producing cell showed a 3-fold increase in productivity, while the light-generating cell could emit light even after 24 h, ~4-fold brighter light than the system without XR/lactose. Levels of acetyl-CoA, NADPH, and ATP were found to be higher in the XR/lactose systems in both fatty alcohol and light-generating cells because both systems require high utilization of these cofactors. Interestingly, only the light-generating cells showed an increase of FMN because this cofactor is required for the function of LuxAB.

For the single-step bioconversion, as for the case of *E. coli* containing FAP, our results revealed that only FAD was found as a cofactor prominently changed in this cell type. The amount of FAD in the cell using XR/lactose was around 3-fold higher than in the control cell. The alkane productivity was improved by 2-fold.

Among the metabolites detected by the untargeted metabolomics approach, S6P/Gal1P and tagatose 1,6-bisphosphate, the products of sorbitol and galactitol metabolic pathways which can enter glycolysis, existed in all cells with similar time-course kinetics of production. The data suggest that the XR cell can convert D-glucose and D-galactose to the corresponding sugar alcohols efficiently and simultaneously. Interestingly, the changes of metabolites in the XR cell are according to the cell-specific demand. Without utilization, the XR cell does not increase cofactors universally. Due to their activities in the sugar metabolic pathways, the XR/lactose system also increased cellular levels of metabolites required for alleviating cellular stress such as glutathione and CoA disulfide, thus increasing cell fitness and allowing the XR-incorporated cell to tolerate to H<sub>2</sub>O<sub>2</sub> better. Therefore, the XR/lactose system is a simple and useful technology for enhancing cell fitness for bioproduction.

The use of the XR/lactose system is different from previous engineering efforts to increase cellular cofactors which generally involved manipulation of several genes in central metabolic pathways (9, 39, 40). The genetic modifications for boosting cofactors production are not always successful due to several disturbances of metabolic pathway largely in central carbon metabolisms which resulting in deteriorate cell growth. Furthermore, functions of those cofactors in metabolic network make genetic engineering entangling.

It should be noted that the XR/lactose used here is not the same as earlier studies of cells harboring XR. Most studies employed XR in combination with xylose (41–43) to reduce xylose to xylitol which is a valuable compound. Sun and colleagues (43) co-expressed acetyl-CoA synthase with XR, xylitol dehydrogenase, and xylulose kinase in *Saccharomyces cerevisiae* to enable the co-utilization of xylose and acetate as a

carbon source. It was interesting to note that in the previous study in which XR was incorporated into cells harboring the  $\alpha,\omega$ -dicarboxylic acids (DCA) pathway to produce DCA from tetradecanoic acid in *E. coli*, the DCA titer was increased by 1.8-fold. No clear reasons were available then.

In conclusion, our findings suggest that the XR/lactose system can be used as a simple synthetic biology tool to enhance levels of sugar phosphates which lead to *in situ* generation of various cofactors upon cellular demand (Fig. 10). The synthesis of specific cofactors depends on cellular usage of overexpressed metabolic pathways. As the demand for cellular cofactors is dynamic, our approach of increasing precursor pools of sugar-phosphates would reduce the metabolic burden and eliminate cofactor imbalance in the metabolically engineered cells.

## Experimental procedures

### Chemicals and reagents

All commercially available chemicals were purchased from Agilent, Sigma-Aldrich, TCI, or Merck. T4 DNA ligase, Restriction enzymes, PCR kits, Gibson assembly kits, and other molecular biology reagents were purchased from New England Biolabs (NEB). Plasmid extraction mini kit and Gel/PCR mini kit were purchased from Favogen Biotech Corporations.

### Strains and plasmids

BL21 (DE3) (*fhuA2 [lon] ompT gal ( $\lambda$  DE3) [dcm]  $\Delta$ hdsS)* cells from Novagen was used for protein expression. The pET28a, pETDuet-1, pRSFDuet-1, and pCDFDuet-1 vectors (Novagen) were used for construction of expression plasmids. Every gene on the pET28a and Duet-1 vector was controlled by the T7 ribosome binding site sequence, AAGGAG. The preparation of expression plasmids used in this study is described below. All engineered *E. coli* strains are listed in Table S4.

### Construction of pETDuet-*mbp-far*, pETDuet-*mbp-far-gst-xr*, and pETDuet-*mbp-far-gdh*

For construction of pETDuet-*mbp-far* plasmid, a gene encoding for a fusion protein of maltose binding protein-fatty acyl coA reductase (FAR) from *Marinobacter aquaeolei* VT8 was amplified with the primers F-lacI and F-M13 (Table S5) using pMAL-*mbp-far* as a template. The *mbp-far* gene was codon-optimized, synthesized, and supplied on a pMAL plasmid by Genscript. The resulting PCR product was digested with *Nde*I and ligated with the *Nde*I/*Eco*RV cut pETDuet-1 vector to yield the pETDuet-*mbp-far* plasmid. For construction of the pETDuet-*mbp-far-gst-xr* plasmid, the pETDuet-*mbp-far* was digested with *Not*I/*Nco*I and ligated with the PCR product of *gst-xr* genes using the Gibson assembly kit. The *gst-xr* from *H. jecorina* gene was codon-optimized, synthesized, and supplied on a pGEX-4T plasmid by Genscript. The primers F-*gst-xr* and R-*gst-xr* (Table S5) were used to amplify the *gst-xr* gene using the pGEX-*gst-xr* as a template. The glucose dehydrogenase (*gdh*) gene from *Bacillus amyloliquefaciens* SB5 was previously constructed in the pJET1.2/blunt-

## XR and lactose boost microbial cofactor synthesis

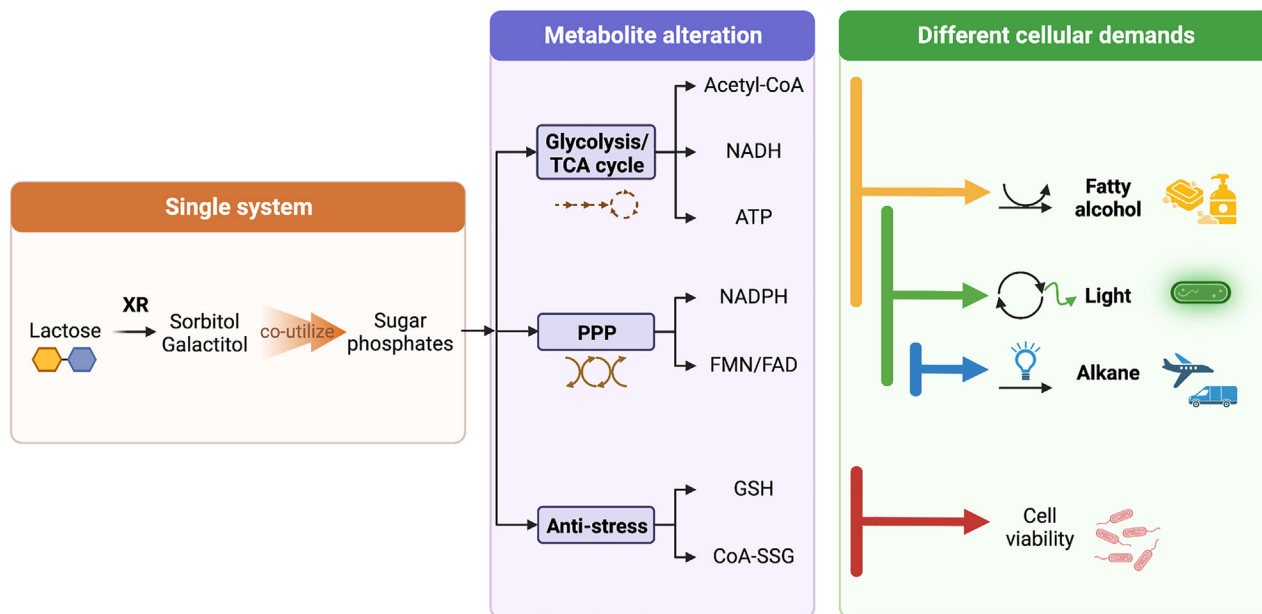


**Figure 10.** A summary of the XR/lactose system, a simple synthetic biology tool for increasing sugar phosphate levels and producing different cofactors on demand. XR/lactose, xylose reductase/lactose.

end cloning vector (44). The primers F-ATG-6XHis-gdh and R-ATG-6XHis-gdh (Table S5) were used to amplify the *gdh* gene and subcloned into pRSFDuet-1 using the Gibson assembly kit at *NcoI* and *NotI* sites to yield the pRSFDuet-6xHis-*gdh* plasmid. For construction of pETDuet-*mbp-far-gdh*, pRSFDuet-6xHis-*gdh* was digested and the resulting fragment was ligated into pETDuet-*mbp-far* at *ApaI* and *NdeI* cutting sites (Fig. S8).

### Construction of pETDuet-luxCDEAB

For construction of the pETDuet-*luxCDEAB* plasmid, genes encoding for LuxCDE and LuxAB from *Vibrio campbellii* were amplified with the primers F-luxCDE and R-luxCDE and primers F-luxAB and R-luxAB, respectively (Table S5). pET17b-*VcluxCDE* and pET11a-*VcluxAB* plasmids were used as templates for amplification. The resulting PCR product of *luxAB* was digested with *NdeI/XhoI* and ligated with the *NdeI/XhoI* digested pETDuet-1 vector to yield the pETDuet-*luxAB* plasmid. The resulting pETDuet-*luxAB* was cut with *BamHI/NcoI* and ligated with *luxCDE* PCR product using Gibson assembly kit to yield the pETDuet-*luxCDEAB* plasmid (Fig. S8).

### Construction of pRSFDuet-gst-xr

For construction of the pRSFDuet-*gst-xr* plasmid, a codon optimized *gst-xr* from *H. jecorina* was amplified with the primers F-pRSF-xr and R-pRSF-xr (Table S5) using pGEX-*gst-xr* as a template. The resulting PCR product was ligated with *NdeI* digested pRSFDuet-1 vector using a Gibson assembly kit to yield the pRSFDuet-*gst-xr* plasmid (Fig. S8).

### Construction of pET28a-fap and pCDFDuet-fap

pET28a-*fap* plasmid was prepared according to previous reports (45, 46). Briefly, cDNA encoding FAP from *Chlorella variabilis* (*Cvfap*) was cloned, amplified by excluding predicted

targeting sequence for chloroplasts, and codon-optimized for expression in *E. coli* and ligated into the pLIC07 vector. The gene cassette consists of 6xHis-tagged, thioredoxin, a tobacco etch virus protease cleavage site, and a gene encoding for *Cvfap*. This construct was cloned into pET28a between *NdeI/HindIII* sites to generate pET28a-*fap*. For construction of the pCDFDuet-*fap* plasmid, pET28a-*fap* was cut with *NdeI* and *XhoI* to generate a fragment consisting of 6xHis-tagged, thioredoxin, tobacco etch virus protease cleavage site, and *Cvfap*. This fragment was inserted into the second multiple cloning site (MSC-2) of pCDFDuet-1 between *NdeI/XhoI* sites by T4 DNA ligase (Fig. S8).

### Construction of *E. coli* BL21 (DE3), *glmS::pT7-gst-xr*, *Gm<sup>r</sup>*

To construct *E. coli* BL21 (DE3), *glmS::pT7-gst-xr*, *Gm<sup>r</sup>* strain, the pT7-*gst-xr* fragment was amplified with the primers F-pT7-*gst-xr* and R-pT7-*gst-xr* (Table S5) using pETDuet-*mbp-far-gst-xr* as a template. This PCR fragment was ligated with *SmaI* cut pUC18T-mini-*Tn7T-Gm<sup>r</sup>-R6K*, generating pUC18T-mini-*Tn7T-Gm<sup>r</sup>-R6K-pT7-gst-xr*. The resulting pUC18T-mini-*Tn7T-Gm<sup>r</sup>-R6K-pT7-gst-xr* plasmid was used to transform *E. coli* BW20767. *E. coli* BW20767 containing pTNS2 and *E. coli* BW20767 containing pUC18T-mini-*Tn7T-Gm<sup>r</sup>-R6K-pT7-gst-xr* was used to transfer pT7-*gst-xr* into *E. coli* BL21 (DE3) containing the pACYCDuet-1 plasmid by triparental conjugation. *E. coli* transconjugants harboring chromosomal insert of the pT7-*gst-xr* gene at downstream of the *glmS* genes were selected on LB agar plate containing 30 µg/ml gentamycin while *E. coli* BW20767 was counter-selected using 15 µg/ml chloramphenicol. The *E. coli* BL21 (DE3), *glmS::pT7-gst-xr*, *Gm<sup>r</sup>* strain was subsequently streaked on an LB agar plate containing 30 µg/ml gentamycin for ten passages for removing the pACYCDuet-1 plasmid. Colony

PCR was used to identify clones with the insertion of pT7-*gst-xr* on the chromosome.

### Preparation of fatty alcohol producing cells and bioconversion assays

The pETDuet-*mbp-far* plasmid was transformed into competent *E. coli* BL21 (DE3) with 15 ng of plasmid to generate the engineered cell without *xr*. The pETDuet-*mbp-far-gst-xr* plasmid was transformed into competent *E. coli* BL21 (DE3) with 15 ng of plasmid to generate the engineered cell with *xr*. The pETDuet-*mbp-far-gdh* plasmid was transformed into competent *E. coli* BL21 (DE3) with 15 ng of plasmid to generate the engineered cell with *gdh*. The transformed cells were selected by growth on LB with 100 µg/ml ampicillin. A single colony was selected and grown in LB with 100 µg/ml ampicillin as a starting liquid culture overnight at 37 °C. The corresponding variant was then sub-cultured into TB or modified M9 media (M9 salt + 33 mM thiamine, 0.1% (w/v) casamino acids (as amino acids source), 0.2% (v/v) glycerol (as carbon source)) with 1% inoculant (by volume) and grown at 37 °C until the OD<sub>600</sub> reached 0.6. The culture was then induced with 1 mM lactose and incubated further at 25 °C for 6 h. Bacterial cells were harvested by centrifugation at 4 °C, and then resuspended in 0.1 M potassium phosphate (Kpi) buffer pH 7.5 to obtain a cell suspension with OD<sub>600</sub> of 30 for 1 ml. This suspension was used for biocatalytic reactions. Various sugars including 20 mM glucose, 10 mM glucose/10 mM arabinose, 10 mM glucose/10 mM fructose, 10 mM glucose/10 mM galactose, and 10 mM lactose were used as carbon sources. The reactions were incubated at 220 rpm, 25 °C. The biocatalytic reaction (1 ml) was carried out in a gas tight vial for designated periods of time and quenched by adding 2 ml ethyl acetate solvent containing internal standards (200 µM tetradecane) with vigorous mixing. Upon addition of ethyl acetate, the mixture was centrifuged (4 °C, 3900g, 20 min) to enhance phase separation and the upper organic layer was analyzed by Agilent7890B GC-MS equipped with a HP5-MS column. The samples for sugar and gene expression analysis (100 µl) were collected from the reaction and centrifuged at 4000g at 4 °C for 10 min. For intra- and extracellular sugar analysis, cell pellet and supernatant were separated and kept at -20 °C. For gene expression analysis, only cell pellet was snap-frozen in liquid nitrogen and kept at -80 °C until further analysis.

### Light generating cell preparation and light measurement

The pETDuet-*luxCDEAB* plasmid was transformed into competent *E. coli* BL21 (DE3) with 15 ng of plasmid to generate the engineered cell without *xr*. The transformed cells were selected by growing on LB with 100 µg/ml ampicillin. The pETDuet-*luxCDEAB* plasmid and pRSFDuet-*gst-xr* plasmid were co-transformed into competent *E. coli* BL21 (DE3) with 15 ng of each plasmid to generate the engineered cell with *xr*. The transformed cells were selected by growing on LB with 100 µg/ml ampicillin and 34 µg/ml kanamycin. A

## ***XR and lactose boost microbial cofactor synthesis***

single colony was selected and grown in LB or modified M9 media with appropriate antibiotic mentioned above as a starting liquid culture overnight at 37 °C. The corresponding variant was then sub-cultured into LB media with 1% inoculant (by volume) and grown at 37 °C until the OD<sub>600</sub> reached 1.0. The culture was then induced with 10 mM lactose and incubated further at 25 °C for 24 h. Bacterial cells were harvested at designated times (0, 2, 4, 8, 12, 24 h) for measuring bioluminescent light. Relative Light Units (RLUs) were measured using a luminometer (AB-2270 Luminescencer-Octa, ATTO) and normalized with OD<sub>600</sub> (RLU/OD<sub>600</sub>).

### Alkane whole-cell biocatalyst preparation and bioconversion assay

The pET28a-*fap* plasmid was transformed into competent *E. coli* BL21 (DE3) with 20 ng of plasmid to generate the engineered cell without *xr*. The pET28a-*fap* plasmid was transformed into competent *E. coli* BL21 (DE3), *glmS::pT7-gst-xr*, *Gm<sup>r</sup>* with 20 ng of plasmid to generate the engineered cell with *xr*. The transformed cells were selected by growth on LB with 34 µg/ml kanamycin. A single colony was selected and grown in LB with the appropriate antibiotic mentioned above as a starting liquid culture overnight at 37 °C. The corresponding variant was then sub-cultured into TB media with 1% inoculant (by volume) and grown at 37 °C until the OD<sub>600</sub> reached 0.6. The culture was then induced with 75 mM lactose and incubated at 25 °C for 20 h in the dark. The bacterial cells were harvested by centrifugation and resuspended in 0.1 M Kpi buffer pH 7.0 to yield an OD<sub>600</sub> of 60/ml. The cells were handled under red light. Bioconversion was done in 1 ml scale in a 20-ml clear glass capped vial containing 10 mM tetradecanoic acid as a substrate for the reaction. Reactions were illuminated under blue light (PPFD-B 20 µmolphotons/m<sup>2</sup>/s) and shaken at 100 rpm, 25 °C. For alkane and fatty acid analysis, the reactions were extracted using ethyl acetate containing internal standard (200 µM tetradecane). The solvent layer was analyzed by Agilent 8890 GC-FID equipped with a HP5 column.

### Quenching of the samples for intracellular metabolites analysis

The method for quenching was performed following the previously reported protocols (47). Samples (1 ml) were rapidly quenched by adding equal volume of cold 60% methanol/water (-40 °C). The quenched samples were centrifuged for 10 min at 4 °C and 800g. The supernatant was removed, and the pellets were snap frozen in liquid nitrogen and stored at -80 °C until metabolite extraction.

### Intracellular metabolite extraction

Intracellular metabolites were extracted using a cold-methanol method following previous research (47). The pellets were resuspended in 2 ml of cold 100% methanol (-80 °C) (HPLC grade). The samples were frozen in liquid nitrogen and thawed on ice for three cycles for extracting intracellular



## XR and lactose boost microbial cofactor synthesis

metabolites. The suspensions were centrifuged at 18,800g at  $-9^{\circ}\text{C}$  for 30 min. The supernatant was transferred into a new 15 ml falcon tube, frozen in liquid nitrogen, and freeze-dried at  $-80^{\circ}\text{C}$ , 1 mbar, for 16 h. The dried samples were maintained on ice, resuspended in 500  $\mu\text{l}$  of cold 50% ACN/water (HPLC grade), and centrifuged for 30 min at 18,800g and at  $-9^{\circ}\text{C}$ . The supernatant was collected and stored at  $-80^{\circ}\text{C}$  until analyzing with mass spectrometry.

### Mass spectrometry analysis

Samples (3  $\mu\text{l}$ ) were injected into an ion mobility drift tube-quadrupole time-of-flight mass spectrometer (LC-IM-QTOF, Agilent 1290 series LC 6560). An Agilent Poroshell 120 HILIC-Z, 2.1 x 150 mm, 2.7  $\mu\text{m}$  (particle size) column was used to achieve optimal separation of metabolites. The flow was 0.3 ml/min with a mobile phase of 10 mM ammonium acetate in water pH 9.0 containing 2.5  $\mu\text{M}$  deactivator (Mobile phase A) and 10 mM ammonium acetate in 85% ACN pH 9.0 containing 2.5  $\mu\text{M}$  deactivator (Mobile phase B). The gradient was changed from 4% of mobile phase A/96% of mobile phase B to 35% of mobile phase A/65% of mobile phase B in 24 min and the column was maintained at  $35^{\circ}\text{C}$ . Data acquisition was performed in IM-QTOF mode. The mass spectrometer was operated in negative ion mode. MS parameters were as follows: gas temperature,  $250^{\circ}\text{C}$ ; sheath gas temperature,  $300^{\circ}\text{C}$ ; sheath gas flow, 12 L/min; fragmentor, 350 V; nozzle voltage, 1000 V; nebulizer, 45 psi; Vcap, 3000 V. The TOF mass was set as  $m/z$  50 to 1700. For ion mobility parameters, high pure nitrogen ( $\text{N}_2$ ) was used for the drift gas. Other IM parameters were set as follows: IM-MS acquisition rate, 1 frame/s and 19 IM transients/frame; entrance and exit voltages of drift tube, 1600 and 250 V; trap filling and trap release times, 3200 and 250  $\mu\text{s}$ ; the drift tube pressure, 3.95 Torr. The drift time was limited to not more than 50 ms. The CCS values were calculated with the single electric field method. All data acquisitions were carried out using MassHunter Workstation Data Acquisition Software (Version B.08.00, Agilent Technologies).

### Data processing and metabolite annotation

Data obtained from LC-IM-QTOF were preprocessed following the previously reported protocols (48). Raw MS data files (.d) were first demultiplexed using the Agilent Demultiplexing tool (Version 1.0, Agilent Technologies). The demultiplexing data files (.DeMP.d) were recalibrated using IM-MS Reprocessor (Version B.08.00, Agilent Technologies). The reference masses used for mass calibration were  $m/z$  112.985587 and 1033.988109. The CCS calibration was performed by the IM-MS Browser software (Version 10.0, Agilent Technologies). The preprocessed data files were submitted for feature finding, alignment, and mass spectra extraction using Mass Profiler (Version 10.0, Agilent Technologies). Finally, the peak table and mass spectra (CEF format) files were exported for statistical analysis and metabolite annotation using Mass profiler professional (Version 15.1, Agilent Technologies) and ID browser identification (Version 10.0, Agilent Technologies), respectively.

The detailed parameters of data processing tools were provided in Table S6. The metabolites were annotated using the parameters of accurate mass, isotope ratios, abundances and spacing, CCS, and retention time matching to standards. The  $m/z$  and CCS tolerance were set at 35 ppm and 5%, respectively.  $[\text{M}-\text{H}]^{-}$ ,  $[\text{M}+\text{CH}_3\text{COO}]^{-}$ ,  $[\text{M}-2\text{H}]^{2-}$ ,  $[\text{2M}+\text{CH}_3\text{COO}]^{-}$ , and  $[\text{2M}-\text{H}]^{-}$  adducts were considered for negative modes. The metabolite databases (METLIN, AICCS (48), HMDB (49), MetCCS (50)) were used for known and unknown metabolite annotation.

Metabolomics data from our work have been deposited in the Metabolomics Workbench (51) (<https://www.metabolomicsworkbench.org>, Project ID PR001849). The data can be retrieved via DOI: <https://doi.org/10.21228/M8QB0V>.

### Statistical analysis

The data files in CEF format were imported to MPP for statistical analysis and visualization. Three separate projects (fatty alcohol, bioluminescence light, and alkane) were created in MPP. Under each project the data files were  $\log_2$  transformed, normalized to total abundance of all samples, and baselined to the median of all samples. The features found in the data file were filtered based on frequency (Table S6) and on sample variability (Coefficient of variation  $\geq 20\%$ ). Unsupervised PCA was performed with mean centering and scaling to display the variance between the two groups (two strains of engineered cells: with and without XR). Statistical evaluation of the data was performed using univariate analyses (52). A cutoff value of  $p < 0.05$  was considered statistically significant in unpaired  $t$  test, using the Benjamini and Hochberg False Discovery Rate set to 5% for multiple testing corrections.

### Intra- and extra-cellular sugar analysis

Concentrations of lactose, glucose, galactose, sorbitol, and galactitol were measured overtime during the bioconversion to produce fatty alcohol (both intracellular and those excreted into the buffer solution). For intracellular sugar analysis, cell pellet was resuspended in water and lysed by ultrasonication. Proteins and cell debris were precipitated with 0.15% formic acid and centrifuged at 18,800g at  $4^{\circ}\text{C}$  for 20 min. The resulting supernatant was filtered by a membrane with pore size 0.22  $\mu\text{m}$  and kept at  $-20^{\circ}\text{C}$  until further analysis. Sugars were identified and measured by LC-triple quadrupole mass spectrometry Agilent 1200 series LC 6470. The Agilent Hilex H, 7.7 x 300 mm column operated at  $35^{\circ}\text{C}$  was used to achieve optimal separation. The flow rate was 0.3 ml/min using an isocratic mobile phase of 0.1% formic acid in water. The mass spectrometer was operated in a negative selective ion monitoring mode to detect sugar and sugar alcohol based on the parameters of retention time and  $m/z$  by comparison to the values of standard compounds. MS parameters were as follows: gas temperature,  $250^{\circ}\text{C}$ ; gas flow, 12 L/min; nebulizer, 45 psi; sheath gas flow, 12 L/min; capillary voltage, 3000 V; and VCharging, 1000.

### Gene expression analysis by quantitative real-time PCR

To identify the up-regulated genes in the engineered XR-harboring cells in accordance with untargeted metabolomics analysis, the fatty alcohol biocatalyst during the bioconversion process was subjected to analysis of gene expression. Total RNA was extracted from the cell pellet by hot acid-phenol/chloroform method and converted into complementary DNA (cDNA) by reverse transcription. The quantitative real-time PCR was performed using KAPA SYBR FAST qPCR Master Mix (2X) Kit (KAPA Biosystems) with StepOnePlus Real-Time PCR system (Applied Biosystems). The gene expression level was calculated by  $\Delta\Delta C_t$  method normalized with the *16s rRNA* gene and compared relative to those from the reference sample. Primers for PCR were listed in Table S7. Multiple unpaired *t* test was used to compare a mean of each target gene from different strains by GraphPad Prism version 9.3.1 (GraphPad Software). The cutoff value of  $p < 0.05$  was adjusted for multiple comparisons using Bonferroni-Dunn method and considered as statistically significant different.

### Data availability

All data are contained in the manuscript or [Supporting information](#).

**Supporting information**—This article contains supporting information.

**Author contributions**—J. J., C. S., and P. C. conceptualization; J. J., C. S., J. P., W. C., C. K., N. A., N. K., K. P., S. A., and M. F. investigation; J. J., C. S., J. P., W. C., C. K., N. A., and N. K. methodology; J. J., C. S., K. P., S. A., and M. F. formal analysis; T. P. and F. H. resources; J. J., C. S., and P. C. writing—original draft; J. J., C. S., and P. C. writing—review and editing.

**Funding and additional information**—This research was financially supported by The Thailand Science Research Innovation NSRF via the Program Management Unit for Human Resources & Institutional Development, Research and Innovation [grant number B05F640089], Kasikornbank, PTT public company limited, Bangkok Industrial Gas, TSRI fundamental fund, and Vidyasirimedhi Institute of Science and Technology (VISTEC) (to J. J., C. S., J. P., W. C., C. K., N. A., N. K., and P. C.).

**Conflict of interest**—The authors declare that they have no conflicts of interest with the contents of this article.

**Abbreviations**—The abbreviations used are: 3-PG, 3-Phosphoglycerate; 4R5AU, 5-Amino-6-(1-D-ribitylamino) uracil; 5-MeTHF, 5-Methyltetrahydrofuran; 6-PG, 6-Phosphogluconic acid; *cysK*, Cysteine synthase; DCA,  $\alpha,\omega$ -dicarboxylic acid; FAP, Fatty acid photodecarboxylase; FAR, Fatty-acyl ACP/CoA reductase; FMN, Flavin mononucleotide; G6P, Glucose-6-phosphate; Gal1P, Galactitol-1-phosphate; *gdh*, NADP<sup>+</sup>-dependent glucose dehydrogenase; *gntK*, D-Gluconate kinase; *gor*, Glutathione reductase; GSH, Glutathione; *gshB*, Glutathione synthetase; *hisC*, Histidinol-phosphate aminotransferase; KAPA, 7-Keto-8-aminopelargonic acid; Lux-CDEAB, Bacterial luciferase; PCA, principal component analysis;

S6P, Sorbitol-6-phosphate; XR, Xylose reductase; *zwf*, NADP<sup>+</sup>-dependent glucose-6-phosphate dehydrogenase.

### References

- Intasian, P., Prakinee, K., Phintha, A., Trisrivirat, D., Weeranoppanant, N., Wongnate, T., *et al.* (2021) Enzymes, *in vivo* biocatalysis, and metabolic engineering for enabling a circular economy and sustainability. *Chem. Rev.* **121**, 10367–10451
- Yilmaz, S., Nyerges, A., van der Oost, J., Church, G. M., and Claassens, N. J. (2022) Towards next-generation cell factories by rational genome-scale engineering. *Nat. Catal.* **5**, 751–765
- Lee, S. Y., Kim, H. U., Chae, T. U., Cho, J. S., Kim, J. W., Shin, J. H., *et al.* (2019) A comprehensive metabolic map for production of bio-based chemicals. *Nat. Catal.* **2**, 18–33
- Bell, E. L., Finnigan, W., France, S. P., Green, A. P., Hayes, M. A., Hepworth, L. J., *et al.* (2021) Biocatalysis. *Nat. Rev. Methods Primers* **1**, 46
- Wu, S., Snajdrova, R., Moore, J. C., Baldenius, K., and Bornscheuer, U. T. (2021) Biocatalysis: enzymatic synthesis for industrial applications. *Angew. Chem. Int. Ed.* **60**, 88–119
- Kim, M., Elvin, C., Brownlee, A., and Lyons, R. (2007) High yield expression of recombinant pro-resilin: lactose-induced fermentation in *E. coli* and facile purification. *Protein Expr. Purif.* **52**, 230–236
- Moon, Y. M., Yang, S. Y., Choi, T. R., Jung, H. R., Song, H. S., Han, Y. H., *et al.* (2019) Enhanced production of cadaverine by the addition of hexadecyltrimethylammonium bromide to whole cell system with regeneration of pyridoxal-5'-phosphate and ATP. *Enzyme Microb. Technol.* **127**, 58–64
- Soo-Yeon, Y., Yeong-Hoon, H., Ye-Lim, P., Jun-Young, P., So-young, N., Daham, J., *et al.* (2020) Production of L-theanine using *Escherichia coli* whole-cell overexpressing  $\gamma$ -glutamylmethylamide synthetase with Baker's yeast. *J. Microbiol. Biotechnol.* **30**, 785–792
- Satowa, D., Fujiwara, R., Uchio, S., Nakano, M., Otomo, C., Hirata, Y., *et al.* (2020) Metabolic engineering of *E. coli* for improving mevalonate production to promote NADPH regeneration and enhance acetyl-CoA supply. *Biotechnol. Bioeng.* **117**, 2153–2164
- Zhao, H., and van der Donk, W. A. (2003) Regeneration of cofactors for use in biocatalysis. *Curr. Opin. Biotechnol.* **14**, 583–589
- Schrewe, M., Julsing, M. K., Buhler, B., and Schmid, A. (2013) Whole-cell biocatalysis for selective and productive C–O functional group introduction and modification. *Chem. Soc. Rev.* **42**, 6346–6377
- Liu, J., Li, H., Zhao, G., Caiyin, Q., and Qiao, J. (2018) Redox cofactor engineering in industrial microorganisms: strategies, recent applications and future directions. *J. Ind. Microbiol. Biotechnol.* **45**, 313–327
- Groger, H., Chamouveau, F., Orologas, N., Rollmann, C., Drauz, K., Hummel, W., *et al.* (2006) Enantioselective reduction of ketones with “designer cells” at high substrate concentrations: highly efficient access to functionalized optically active alcohols. *Angew. Chem. Int. Ed.* **45**, 5677–5681
- Ernst, M., Kaup, B., Müller, M., Bringer-Meyer, S., and Sahm, H. (2005) Enantioselective reduction of carbonyl compounds by whole-cell biotransformation, combining a formate dehydrogenase and a (R)-specific alcohol dehydrogenase. *Appl. Microbiol. Biotechnol.* **66**, 629–634
- Pan, X., Yu, J., Du, Q., Zeng, S., Liu, J., Jiao, Q., *et al.* (2020) Efficient synthesis of gamma-glutamyl compounds by co-expression of gamma-glutamylmethylamide synthetase and polyphosphate kinase in engineered *Escherichia coli*. *J. Ind. Microbiol. Biotechnol.* **47**, 573–583
- Zhao, J., Li, Q., Sun, T., Zhu, X., Xu, H., Tang, J., *et al.* (2013) Engineering central metabolic modules of *Escherichia coli* for improving beta-carotene production. *Metab. Eng.* **17**, 42–50
- Diaz, C. A. C., Bennett, R. K., Papoutsakis, E. T., and Antoniewicz, M. R. (2019) Deletion of four genes in *Escherichia coli* enables preferential consumption of xylose and secretion of glucose. *Metab. Eng.* **52**, 168–177
- Siedler, S., Bringer, S., and Bott, M. (2011) Increased NADPH availability in *Escherichia coli*: improvement of the product per glucose ratio in reductive whole-cell biotransformation. *Appl. Microbiol. Biotechnol.* **92**, 929–937



19. Feng, X., and Zhao, H. (2013) Investigating xylose metabolism in recombinant *Saccharomyces cerevisiae* via <sup>13</sup>C metabolic flux analysis. *Microb. Cell Fact.* **12**, 114
20. Yuan, X., Wang, J., Lin, J., Yang, L., and Wu, M. (2019) Efficient production of xylitol by the integration of multiple copies of xylose reductase gene and the deletion of Embden–Meyerhof–Parnas pathway-associated genes to enhance NADPH regeneration in *Escherichia coli*. *J. Ind. Microbiol. Biotechnol.* **46**, 1061–1069
21. Chin, J. W., and Cirino, P. C. (2011) Improved NADPH supply for xylitol production by engineered *Escherichia coli* with glycolytic mutations. *Biotechnol. Prog.* **27**, 333–341
22. Donovan, R. S., Robinson, C. W., and Glick, B. R. (2000) Optimizing the expression of a monoclonal antibody fragment under the transcriptional control of the *Escherichia coli* lac promoter. *Can. J. Microbiol.* **46**, 532–541
23. Kotik, M., Kocanová, M., Maresová, H., and Kyslík, P. (2004) High-level expression of a fungal pyranose oxidase in high cell-density fed-batch cultivations of *Escherichia coli* using lactose as inducer. *Protein Expr. Purif.* **36**, 61–69
24. Komeda, H., Yamasaki-Yashiki, S., Hoshino, K., and Asano, Y. (2015) Identification and characterization of D-xylose reductase involved in pentose catabolism of the zygomycetous fungus *Rhizomucor pusillus*. *J. Biosci. Bioeng.* **119**, 57–64
25. Seiboth, B., Gamauf, C., Pail, M., Hartl, L., and Kubicek, C. P. (2007) The d-xylose reductase of *Hypocrea jecorina* is the major aldose reductase in pentose and D-galactose catabolism and necessary for beta-galactosidase and cellulase induction by lactose. *Mol. Microbiol.* **66**, 890–900
26. Biswas, D., Pandya, V., Singh, A. K., Mondal, A. K., and Kumaran, S. (2012) Co-factor binding confers substrate specificity to xylose reductase from *Debaryomyces hansenii*. *PLoS One* **7**, e45525
27. Daegelen, P., Studier, F. W., Lenski, R. E., Cure, S., and Kim, J. F. (2009) Tracing ancestors and relatives of *Escherichia coli* B, and the derivation of B strains REL606 and BL21(DE3). *J. Mol. Biol.* **394**, 634–643
28. Munkajohnpong, P., Kesornpun, C., Buttranon, S., Jaroensuk, J., Weeranoppanant, N., and Chaiyen, P. (2020) Fatty alcohol production: an opportunity of bioprocess. *Biofuels Bioprod. Biorefin.* **14**, 986–1009
29. Zheng, M., Åslund, F., and Storz, G. (1998) Activation of the OxyR transcription factor by reversible disulfide bond formation. *Science* **279**, 1718–1722
30. Smirnova, G. V., Krasnykh, T. A., and Oktyabrsky, O. N. (2001) Role of glutathione in the response of *Escherichia coli* to osmotic stress. *Biochemistry (Mosc)* **66**, 973–978
31. Zhang, Y., Zhang, Y., Zhu, Y., Mao, S., and Li, Y. (2010) Proteomic analyses to reveal the protective role of glutathione in resistance of *Lactococcus lactis* to osmotic stress. *Appl. Environ. Microbiol.* **76**, 3177–3186
32. Styrvold, O. B., and Strom, A. R. (1991) Synthesis, accumulation, and excretion of trehalose in osmotically stressed *Escherichia coli* K-12 strains: influence of amber suppressors and function of the periplasmic trehalase. *J. Bacteriol.* **173**, 1187–1192
33. Zhu, L., Dong, H., Zhang, Y., and Li, Y. (2011) Engineering the robustness of *Clostridium acetobutylicum* by introducing glutathione biosynthetic capability. *Metab. Eng.* **13**, 426–434
34. Tinikul, R., and Chaiyen, P. (2016) Structure, mechanism, and mutation of bacterial luciferase. *Adv. Biochem. Eng. Biotechnol.* **154**, 47–74
35. Lakavath, B., Hedison, T. M., Heyes, D. J., Shanmugam, M., Sakuma, M., Hoeven, R., et al. (2020) Radical-based photoinactivation of fatty acid photodecarboxylases. *Anal. Biochem.* **600**, 113749
36. Wu, Y., Paul, C. E., and Hollmann, F. (2021) Stabilisation of the fatty acid decarboxylase from *Chlorella variabilis* by caprylic acid. *Chembiochem* **22**, 2420–2423
37. Moulin, S., Légeret, B., Blangy, S., Sorigué, D., Burlacot, A., Auroy, P., et al. (2019) Continuous photoproduction of hydrocarbon drop-in fuel by microbial cell factories. *Sci. Rep.* **9**, 13713
38. Li, J., Ma, Y., Liu, N., Eser, B. E., Guo, Z., Jensen, P. R., et al. (2020) Synthesis of high-titer alka(e)nes in *Yarrowia lipolytica* is enabled by a discovered mechanism. *Nat. Commun.* **11**, 6198
39. Li, C., Ying, L. Q., Zhang, S. S., Chen, N., Liu, W. F., and Tao, Y. (2015) Modification of targets related to the Entner–Doudoroff/pentose phosphate pathway route for methyl-D-erythritol 4-phosphate-dependent carotenoid biosynthesis in *Escherichia coli*. *Microb. Cell Fact.* **14**, 117
40. Fujiwara, R., Noda, S., Tanaka, T., and Kondo, A. (2020) Metabolic engineering of *Escherichia coli* for shikimate pathway derivative production from glucose-xylose co-substrate. *Nat. Commun.* **11**, 279
41. Wei, N., Quarterman, J., Kim, S. R., Cate, J. H., and Jin, Y. S. (2013) Enhanced biofuel production through coupled acetic acid and xylose consumption by engineered yeast. *Nat. Commun.* **4**, 2580
42. Sathesh-Prabu, C., and Lee, S. K. (2018) Enhancement of alpha,omega-dicarboxylic acid production by the expression of xylose reductase for refactoring redox cofactor regeneration. *J. Agric. Food Chem.* **66**, 3489–3497
43. Sun, L., Lee, J. W., Yook, S., Lane, S., Sun, Z., Kim, S. R., et al. (2021) Complete and efficient conversion of plant cell wall hemicellulose into high-value bioproducts by engineered yeast. *Nat. Commun.* **12**, 4975
44. Pongtharangkul, T., Chuekitkumchorn, P., Suwanampa, N., Payongsri, P., Honda, K., and Panbangred, W. (2015) Kinetic properties and stability of glucose dehydrogenase from *Bacillus amyloliquefaciens* SB5 and its potential for cofactor regeneration. *AMB Express* **5**, 68
45. Huijbers, M. M. E., Zhang, W., Tonin, F., and Hollmann, F. (2018) Light-driven enzymatic decarboxylation of fatty acids. *Angew. Chem. Int. Ed. Engl.* **57**, 13648–13651
46. Sorigué, D., Légeret, B., Cuiñé, S., Blangy, S., Moulin, S., Billon, E., et al. (2017) An algal photoenzyme converts fatty acids to hydrocarbons. *Science* **357**, 903–907
47. Winder, C. L., Dunn, W. B., Schuler, S., Broadhurst, D., Jarvis, R., Stephens, G. M., et al. (2008) Global metabolic profiling of *Escherichia coli* cultures: an evaluation of methods for quenching and extraction of intracellular metabolites. *Anal. Chem.* **80**, 2939–2948
48. Zhou, Z., Luo, M., Chen, X., Yin, Y., Xiong, X., Wang, R., et al. (2020) Ion mobility collision cross-section atlas for known and unknown metabolite annotation in untargeted metabolomics. *Nat. Commun.* **11**, 4334
49. Wishart, D. S., Guo, A., Oler, E., Wang, F., Anjum, A., Peters, H., et al. (2022) Hmdb 5.0: the human metabolome database for 2022. *Nucleic Acids Res.* **50**, D622–D631
50. Zhou, Z., Shen, X., Tu, J., and Zhu, Z. J. (2016) Large-scale prediction of collision cross-section values for metabolites in ion mobility-mass spectrometry. *Anal. Chem.* **88**, 11084–11091
51. Sud, M., Fahy, E., Cotter, D., Azam, K., Vadivelu, I., Burant, C., et al. (2016) Metabolomics workbench: an international repository for metabolomics data and metadata, metabolite standards, protocols, tutorials and training, and analysis tools. *Nucleic Acids Res.* **44**, D463–D470
52. Vinaixa, M., Samino, S., Saez, I., Duran, J., Guinovart, J. J., and Yanes, O. (2012) A guideline to univariate statistical analysis for LC/MS-based untargeted metabolomics-derived data. *Metabolites* **2**, 775–795